







**Laboratoire de Chimie Théorique UMR 7616**  
**Interprétation Chimique**  
**Dossier pour Habilitation á diriger des recherches en Chimie**

**Revealing Non Covalent Interactions.**

**Analysis and development of the reduced density gradient in molecules  
and solids**

**Rapporteurs: Odile Eisenstein, Christophe Morell and Manuel Yañez.**

**Jury: Odile Eisenstein, Angel Martin Pendas, Christophe Morell, Frank de Proft, Henry S. Rzepa, Bernard  
Silvi and Manuel Yañez.**

Julia Contreras García

October 2015





*This is the story of how chemical albonding me persigue. En 3D.*

# Contents

## Part I My research 1

<b>1</b>	<b>Introduction</b>	<b>3</b>
1.1	Quantum Chemistry and the Chemical Bond	3
1.2	Historical framework	4
1.3	Weak interactions	4
1.3.1	Why do we care about them?	4
1.3.2	The need for a new approach	5
<b>2</b>	<b>NCI: Non-Covalent Interaction index</b>	<b>7</b>
2.1	Constructing NCI	7
2.1.1	The reduced density gradient	7
2.1.2	The electron density	9
2.1.3	The density second eigenvalue	9
2.2	Interpreting NCI	9
2.2.1	The 2D plot	10
2.2.2	The 3D plot	11
2.2.2.1	3D visualization	11
2.2.2.2	2D and 3D shapes	11
2.3	Learn through examples	12
2.3.1	Small molecules	12
2.3.2	Solids	13
2.3.3	Biological Systems	14
2.3.3.1	Promolecular densities	14
2.3.3.2	Examples	15
<b>3</b>	<b>Only weak bonds?</b>	<b>19</b>
3.1	Atomic shells	19
3.2	Ionic bonds	19
3.3	Covalent bonds	21
<b>4</b>	<b>AIM and Beyond</b>	<b>23</b>
4.1	Repulsive BCPs?	23
4.2	Attractive interactions	24
4.2.1	Very weak interactions: missing BCPs?	24
4.2.2	Delocalized interactions: which BCP?	27
4.3	Absence of interaction: too many BCPs	27
<b>5</b>	<b>Software</b>	<b>29</b>

<b>5.1</b>	<b>Molecules</b>	<b>29</b>
5.1.1	Algorithmic details	29
<b>5.2</b>	<b>Solids</b>	<b>31</b>
5.2.1	NCI for solid wavefunctions	31
5.2.1.1	Algorithmic details	31
5.2.1.2	Pseudopotentials	32
5.2.2	NCI for experimental densities	32
5.2.2.1	Algorithmic details	32
<b>6</b>	<b>Energy and NCI</b>	<b>35</b>
6.1	Integration over NCI regions	35
6.2	Hydrogen bonds binding energy curves	35
6.3	Dispersion and additivity	37
6.3.1	The origin of stabilization	37
6.3.2	System size	40
<b>7</b>	<b>Some applications</b>	<b>43</b>
7.1	Reactivity	43
7.2	Chiral recognition	46
<b>8</b>	<b>Summary and conclusions</b>	<b>49</b>
	Bibliography	50
<b>Part II Research Project</b>		<b>53</b>
<b>Part III Curriculum Vitae</b>		<b>59</b>
<b>Part IV Appendix</b>		<b>69</b>



A mis pilares. Sólidos. Inamovibles.  
Qué gran suerte contar con cimientos.

**Part I**  
**My research**



# 1 Introduction

## 1.1

### Quantum Chemistry and the Chemical Bond

As defined by Linus Pauling, “Chemistry is the science of substances: their structure, their properties, and the reactions that change them into other substances”. [1] The first aspects, structure and properties, are clearly associated with the arrangement of atoms in a molecule, i.e. the chemical bond. These bonds determine Pauling’s third aspect, chemical reactivity. In other words, chemical bonds are the undisputed foundation of chemistry and their visualization should allow chemists to understand how molecules behave at the most fundamental level.

Achievement of a mechanistic understanding of chemical and biological functions as well as the structure of solid materials depends on knowing the geometric structure and the nature of bonds. But, despite the “chemical bond” being a fundamental concept in chemistry, **“what is a chemical bond?” still remains a critical question** for the chemical community because of the lack of a unique definition as well as an unclear understanding of its physical nature.

Successful numerical solution of the Schrödinger equation has yielded energies and properties of atoms and molecules, but not yet a clear physical explanation of chemical bonding. There is even a controversy on the mechanistic origin of the most “simple” chemical bond, covalent bonding, as it was remarked by Burdett in his classical book. [2]

As recently as in 2007, a special issue was devoted to the “90 Years of Chemical Bonding”. [3] In this issue, the chemical bond was compared to a unicorn, “a mythical but useful creature, which brings law and order [· · ·] in an otherwise chaotic and disordered world”. [4] Everyone knows how it looks despite nobody ever having seen one. [4–6] This line of reasoning is similar to Coulson’s comment: “Sometimes it seems to me that a bond between two atoms has become so real, so tangible, so friendly, that I can almost see it. Then I awake with a little shock, for a chemical bond is not a real thing. It does not exist. No one has ever seen one. No one ever can. It is a figment of our own imagination.” [7] Even chemical bonds have been described as “noumena” rather than “phenomena”. [8–10]

Chemical bonds together with other concepts such as atomic orbitals, electron shells, lone pairs, aromaticity, atomic charges, (hyper-) conjugation, strain, etc. do not correspond to physical observables. Such concepts therefore cannot be unambiguously defined in pure quantum theory, but constitute a rich set of “fuzzy”, yet invaluablely useful concepts. [11–14] They lead to constructive ideas and developments when appropriately used and defined.

In chemistry as well as in physics, advanced theories are held by two milestones: i) a mathematical structure/formalism disclosing the basic entities of the theory and their mathematical relationships, and ii) an “interpretative” recipe of basic entities of the theory. The latter discloses the qualitative meaning of the basic entities and their relation to other known entities within and beyond the theory. It is important to highlight that the connection between the mathematical formalism and its interpretation is always subtle. This problem can be traced back to the lack of a clear and unambiguous definition of a bond in quantum mechanics and the plethora of interpretations that have been introduced with various “meanings” of the “mathematical symbols/entities” of the theory. [15]

In front of this quandary, two opposite attitudes can be envisaged. On the one hand, the old and negative statement of the French mathematician R. Thom: “Il me faut cependant avouer que la chimie proprement dite ne m’a jamais beaucoup intéressée. Pourquoi? Peut-être parce que des notions telles que celles de valence, de liaison chimique etc., m’ont toujours semblé peu claires du point de vue conceptuel.” (I should admit that chemistry never really interested me. Why? Perhaps because notions such as those of valence, chemical bond, etc., always appeared unclear to me from the conceptual point of view). On the other hand, the more actual and pragmatic comment of Alvarez et al.: “Chemistry has done more than well in a universe of structure and function on the molecular level with just this imperfectly defined concept of a chemical bond. Or maybe it has done so well precisely because the concept is flexible and fuzzy”. [16]

However, it is important to note that scientific arguments, debates, and controversies are at the heart of chemistry. This situation has been clearly stated in the very recent paper entitled “The Nature of the Fourth Bond in the Ground State of C<sub>2</sub>: The Quadruple Bond Conundrum” by Danovich et al., [17] in which these authors recognize that they are in front of a “Rashomon effect”, in which the bonding picture is becoming too fuzzy to be constructive anymore.

## 1.2

### Historical framework

In trying to overcome this dichotomy, different approaches have been developed over the years to reveal chemical bonds. Covalent bonds are intuitively represented using conventional Lewis structures. [19] Molecular Orbital (MO) theory has been very useful and successful for the theoretical analysis of chemical reactions and chemical reactivity. The frontier orbital theory [20] and the orbital symmetry rules of Woodward and Hoffman [21] are paradigmatic examples of the possibilities of quantum chemistry within the MO theory.

To reduce the dimensionality of the problem, three-dimensional interpretative approaches have been introduced. The conceptual density functional theory pioneered by Parr et al. [22] has been at the origin of very useful reactivity descriptors. Another low dimensional approach has originally been developed by Bader: [23–25] the topological approach. Within these approaches, 3D space is divided following the gradient of a scalar function into mutually disjoint regions. Bader’s QTAIM (Quantum Theory of Atoms In Molecules) theory is based on the topological analysis of the density and provides an atomic picture of the system. Chemical bonds and the underlying molecular graph may be traced by the analysis of its bond critical points (BCPs, first order saddle points). Following the same philosophy, ELF [26,27] (Electron Localization Function) topological analysis divides the space into chemically intuitive regions associated with electron pairs so that electronic shells, bonds, and lone pairs are revealed. Also, purely electrostatic interactions can be analyzed using electrostatic potential maps. [28]

## 1.3

### Weak interactions

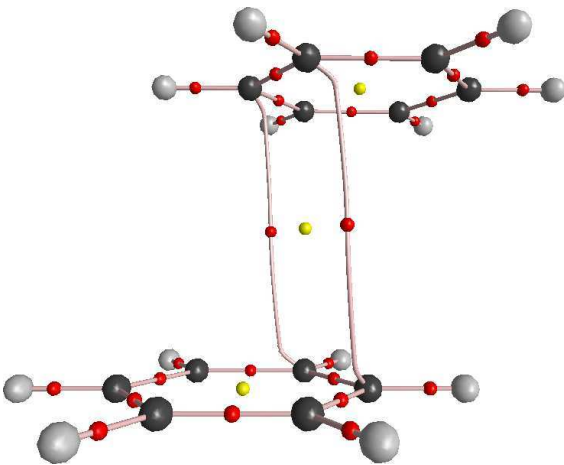
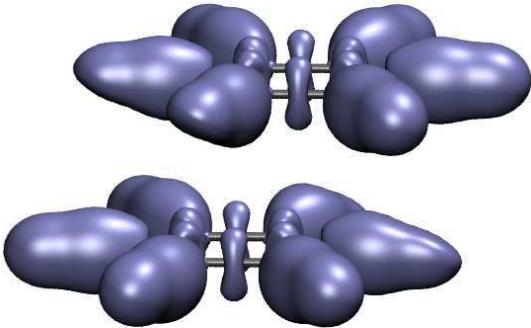
Weak interactions span a wide range of binding energies, and encompasses hydrogen bonding, dipole-dipole interactions and London dispersion [29] as well as more up to date interactions such as halogen bonds, CH $\cdots\pi$  and  $\pi\cdots\pi$  interactions. Repulsive interactions, also known as steric clashes, should not be disregarded either.

#### 1.3.1

##### Why do we care about them?

In spite, or rather because of their weak strength weak interactions are of uttermost importance to our world as we conceive it. Chemical interactions between a protein and a drug, or a catalyst and its substrate,

## 1.1 Comparison between QTAIM and ELF topologies in benzene dimer

Method	QTAIM	ELF
Function Partition	Electron density Atoms	Pauli kinetic energy density Lewis' pairs
Example		 <p style="text-align: center;">ELF=0.9</p>

self-assembly of nanomaterials, [30,31] and even some chemical reactions, [32,33] are dominated by non-covalent interactions.

More specifically, non-covalent interactions are of paramount importance in chemistry and especially in bio-disciplines, [34,35] since they set up the force field scenario through which chemical species interact with each other without a significant electron sharing between them. They represent, in fact, the machinery through which molecules recognize themselves and establish how molecules will approach and eventually pack together.

During the last decade, non-covalent interactions have also raised a great deal of interest in the context of self-assembly [36] and crystallization, [37] whose underlying general rules are at the moment too faraway to be fully rationalized and understood. [38] Knowledge of such rules would in principle allow to build from scratch (even complex) materials exhibiting the desired properties. [30,39,40] Although it can not be ignored that a given observed structure is generally the outcome of a "drawing" among a plethora of energetically similar, but structurally dissimilar options, [41] understanding intermolecular non-covalent interactions and their mutual interplay in the supramolecular assemblies is nonetheless a fundamental step in making progress in structural prediction and evolution.

## 1.3.2

**The need for a new approach**

Non-covalent interactions are frequently visualized using distance-dependent contacts, generally without consideration of hydrogen atoms. [42–44] Hydrogen-bonds can be identified from the molecular geometry [45] and from ELF, [46] while grid-based calculations from classical force fields are used to model other van der Waals interactions. [47] The crucial role of weak interactions can also be analyzed in an indirect manner through property computations (from population to electrostatic moments). [48] However, these fluctuations are not easily visualized. In other words, a visual quantum chemical approach was conspicuously missing in this scenario.

Let's look at an example to clearly pinpoint the state of the art of topological approaches to weak interactions. The image provided by QTAIM and ELF of benzene dimer is provided in Table 1.1. Let's first focus on a given benzene molecule: The electron density shows maxima (cusps) for the C and H atoms, whereas C-H and C-C bonds are represented by BCPs (in red). ELF, instead, provides a picture based on electron localization, so that isosurfaces appear around atoms, C-C and C-H bonds. In both cases the chemical structure is revealed as expected from chemical intuition. However, the ELF picture is obviously more intuitive thanks to the isosurfaces.

Now, if we take a look at the complete system, the stacking dimer, we can see that intermolecular BCPs appear along with a ring critical point (second order saddle point, in yellow). The fact that interactions are related to saddle points, locates them on the interatomic surfaces, so that they highlight interatomic contact, but they do not have an associated region within this approach. Moreover, the critical points unite pairs of C atoms, which is not the chemical picture we have of a stacking interaction: it should appear as a benzene to benzene interaction. The VSEPR regions of benzene dimer are clearly identified by ELF, but nothing is seen for the inter-benzene stacking interaction.

In other words, both approaches fail to correctly provide a picture of delocalized interactions. Thus, it is the aim of this chapter to introduce such a tool, show its advantages over previous theories and its ability to provide a complete and holistic vision of non-covalent interactions and their change directly from the electron density.

## 2 NCI: Non-Covalent Interaction index

The electron density has a fundamental advantage over MO-based descriptors because it is an experimentally accessible scalar field and it is a local function defined within the exact many-body theory, also supported by the Hohenberg-Kohn theorem. [49] The relationship between electron density topology and physical/chemical properties can be understood from the Hohenberg-Kohn theorem, which asserts that a system's ground-state properties are a consequence of its electron density. Furthermore since chemical reactions proceed by  $\rho(\vec{r})$  redistributions, methods that analyze  $\rho(\vec{r})$  distributions should help to understand the electron structure of molecules and thus chemical reactivity (see Section 7.1).

Our approach, introduced in the coming sections, uses the density and its derivatives, allowing simultaneous analysis and visualization of all non-covalent interaction types as real-space surfaces, thus adding an important tool to the chemist's arsenal. [50–52]

### 2.1 Constructing NCI

The Non Covalent Interaction (NCI) index is based on the analysis of the reduced density gradient at low densities in combination with the analysis of the electron density and its derivatives to understand the nature of the interaction.

#### 2.1.1 The reduced density gradient

The reduced density gradient,  $s$ , is a fundamental dimensionless quantity in DFT used to describe the deviation from a homogeneous electron distribution. [49, 53, 54] Properties of the reduced gradient have been investigated in depth in the process of developing increasingly accurate functionals. [55]

The origin of the reduced density gradient can be traced to the generalized gradient contribution to the GGA exchange energy,  $E_X^{GGA}$ , from density-functional theory:

$$E_X^{GGA} - E_X^{LDA} = - \sum \int F(s) \rho^{4/3}(\vec{r}) d\vec{r}, \quad (2.1)$$

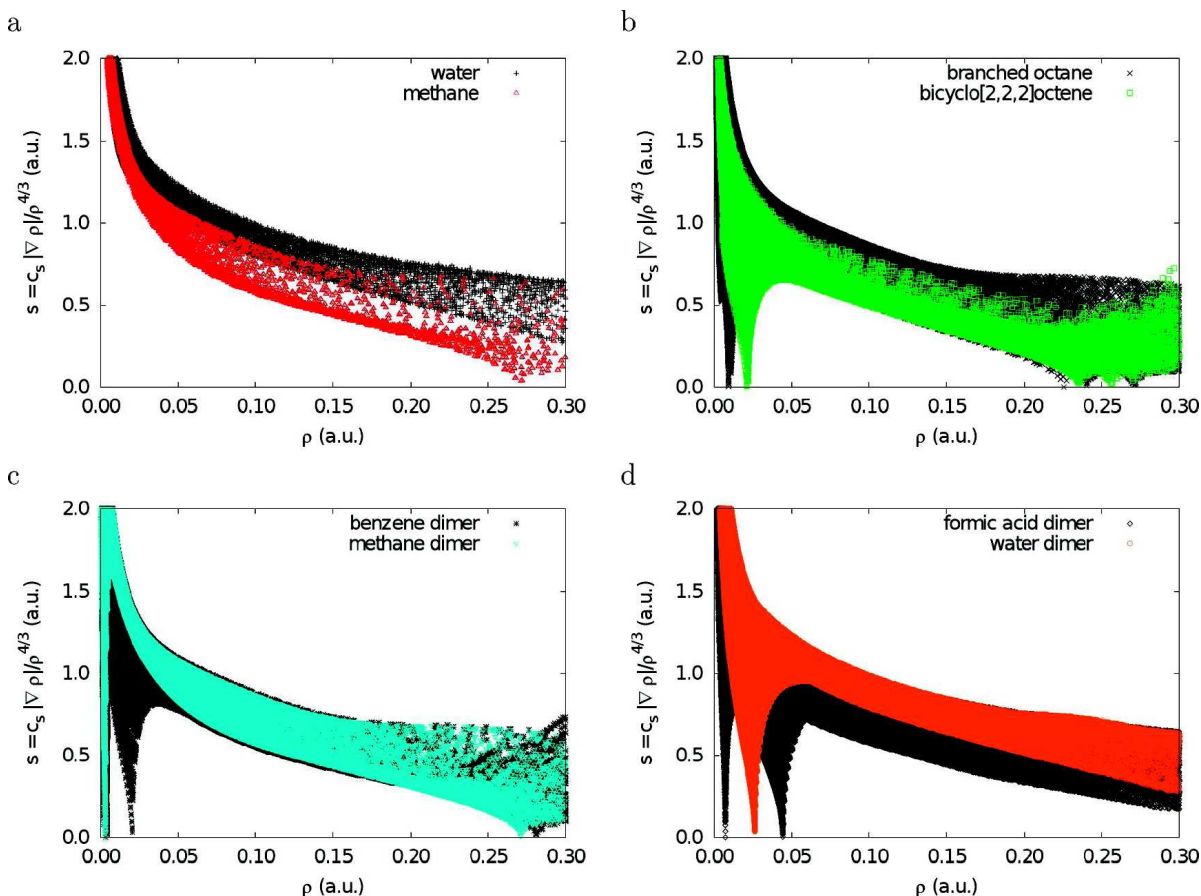
where  $F(s)$  is a function of  $s$  for a given spin with

$$s = \frac{1}{c_F} \frac{|\nabla\rho|}{\rho^{4/3}}, \quad (2.2)$$

$c_F$  being the Fermi constant,  $c_F = 2(3\pi^2)^{1/3}$  and the 4/3 exponent of the density ensuring that  $s$  is a dimensionless quantity.

$s$  accounts for local density inhomogeneities due to its differential behavior depending on the chemical region of the molecule. The reduced density gradient assumes large values in the exponentially-decaying density tails far from the nuclei, where the density denominator approaches zero more rapidly than the gradient numerator. Small values of  $s$  occur close to the nuclei, due to the combination of large densities and small density gradients. The lower bound on the reduced density gradient is zero, as occurs throughout a homogeneous electron gas and at bond critical points.





**2.1** Plots of the electron density and its reduced gradient for methane, water, branched octane, bicyclo [2,2,2]octene, and the homomolecular dimers of methane, benzene, water, and formic acid. The data was obtained by evaluating B3LYP/6-31G\* density and gradient values on cuboid grids, with a 0.1 au step size, for each molecule or dimer. To provide even more sampling of the small low-density, low-gradient regions in hydrogen-bonded complexes, additional calculations were performed for water and formic acid dimers with a much denser 0.025 au grid.

The effect of bonding on the reduced density gradient is especially easy to visualize when  $s$  is plotted as a function of the density. Graphs of  $s(\rho)$  assume the form  $f(x) = ax^{-1/3}$ , where  $a$  is a constant. This can easily be proven from a STO model density. For a single atomic orbital  $\psi = e^{-\alpha r}$ , the density is  $\rho = e^{-2\alpha r}$  and the gradient is  $\nabla\rho = -2\alpha\rho$ , such that

$$s(\rho) = \frac{1}{c_F} \frac{2\alpha\rho}{\rho^{4/3}} = \frac{2\alpha}{c_F} \rho^{-1/3}. \quad (2.3)$$

When there is overlap between atomic orbitals, a spike in the  $s(\rho)$  diagram appears (Figure 2.1). The points forming this spike can identify the interaction when they are mapped back to real space. This procedure is able to reveal non-covalent interactions.

Plotting  $s$  versus  $\rho$ , as in Figure 2.1, reveals the basic pattern of intramolecular interactions. Methane (Figure 2.1a) illustrates the typical covalent bond pattern. The top left-side points (small density and large reduced gradient) correspond to the exponentially-decaying tail regions of the density, far from the nuclei. The points on the bottom right side (density values of ca. 0.25 au and low reduced gradient) correspond to the C-H covalent bonds. Covalent bonds have their characteristic BCP in the electron density, corresponding to  $s = 0$ . Regions near the nuclei have larger density values and appear beyond the right edge of the

plot. The plot has an overall shape of the form  $a\rho^{-1/3}$  because atomic and molecular densities are piecewise exponential. The results for water are very similar, the only difference being that the covalent bonds lie at higher density values, past the edge of the plot. In Figure 2.1b-d, we consider six examples of chemical systems displaying various types of non-covalent interactions. Plots of  $s$  versus  $\rho$  for these systems all exhibit a new feature: one or more spikes in the low-density, low-gradient region, a signature of non-covalent interactions. This is the basis of NCI.

### 2.1.2

#### The electron density

Once the existence of non covalent interactions has been confirmed by the reduced density gradient, it is necessary to separate them in terms of their type. This can be done thanks to the properties of the corresponding critical points. Characteristic densities of van der Waals interactions are much smaller than densities at which hydrogen bonds (HBs) and repulsive clashes appear. Thus, we can use the density to identify the strength of the interactions.

### 2.1.3

#### The density second eigenvalue

However, steric clashes and hydrogen bonds span similar density ranges and overlap in plots of  $s(\rho)$ . We need an extra piece of information to differentiate attractive from repulsive interactions.

According to the divergence theorem, [58] the sign of the Laplacian of the density,  $\nabla^2\rho$ , indicates whether the net gradient flux is entering,  $\nabla^2\rho < 0$ , or leaving,  $\nabla^2\rho > 0$ , an infinitesimal volume around a reference point. Hence, it highlights whether the density is concentrated or depleted at that point, relative to the surrounding environment. To differentiate between different types of weak interactions one cannot resort to the sign of the Laplacian itself (as is common within AIM theory) since it is dominated by the principle axis of variation and is positive for all closed-shell interactions. [59]

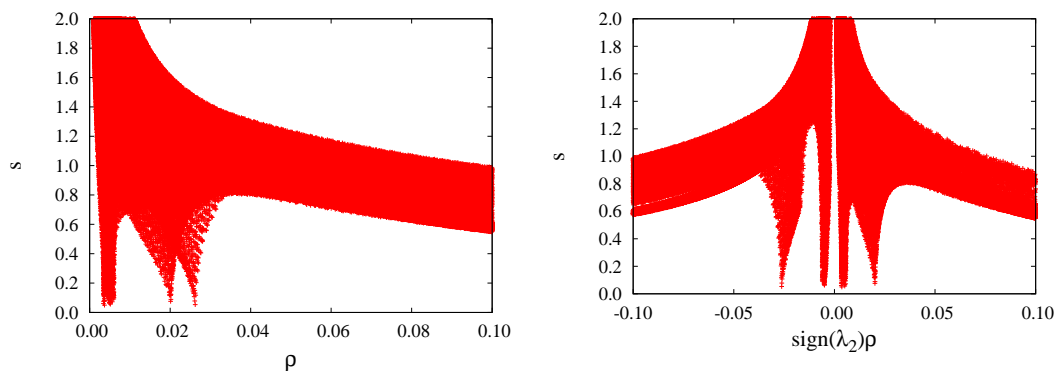
To understand bonding in more detail, it is often useful to decompose the Laplacian into the contributions along the three particular axes of maximal variation. These components are the three eigenvalues  $\lambda_i$  of the electron-density Hessian matrix, such that,  $\nabla^2\rho = \lambda_1 + \lambda_2 + \lambda_3$ , ( $\lambda_1 < \lambda_2 < \lambda_3$ ). At points with zero gradient, analysis of the Hessian eigenvalues is analogous to determining the signature of the critical point. Thus, at nuclei (cusps of  $\rho$  assimilated to maxima), all the eigenvalues are negative, while at the center of cages or holes (minima of  $\rho$ ) all the eigenvalues are positive. In the remaining points of space  $\lambda_3 > 0$ ,  $\lambda_1 < 0$ , and  $\lambda_2$  can be either positive or negative. Within the NCI framework, the sign of  $\lambda_2$  (i.e. the perpendicular plane) enables identification of the interaction type. Attractive interactions appear at  $\lambda_2 < 0$  whereas in the cases where  $\lambda_2$  is positive (as in rings or cages), usually several atoms interact but are not bonded, which corresponds to steric crowding according to classical chemistry.

Both van der Waals interactions and hydrogen bonds show negative values of  $\lambda_2$  at the critical point (with  $\lambda_2 \simeq 0$  for van der Waals interactions). This can be attributed to the homomorphic virial path associated with the bonding direction, which defines a line along which the potential-energy density is maximally negative. Conversely, non-bonding interactions, such as steric crowding, result in density depletion, such that  $\lambda_2 > 0$ . Analogously, the homeomorphism ensures that these critical points (both ring and cages points) identify lines of minimally-negative potential-energy density.

## 2.2

### Interpreting NCI

The reduced density gradient along with the density and its derivatives are united together in two types of representations for the analysis of non covalent interactions: the 2D  $s(\rho)$  plot and the 3D (isosurfaces) plot.



**2.2** Plots of (a)  $s(\rho)$ , (b) NCI isosurface, for the phenol dimer. The  $s = 0.6$  isosurface is colored over the range  $-0.03 < \text{sign}(\lambda_2)\rho < +0.03$  au.

### 2.2.1

#### The 2D plot

The pieces of information,  $s, \rho, \text{sign}(\lambda_2)$  can be put together in a very representative 2D plot derived from the  $s(\rho)$  plots shown above. It suffices to plot  $s$  vs.  $\text{sign}(\lambda_2) \times \rho$  to characterize all non covalent interactions in the system. Thus, the analysis of the sign of  $\lambda_2$  helps to discern between the different types of weak interactions, whereas the density itself provides information about their strength.

This is illustrated for the phenol dimer in Figures 2.2a-b. This is a hydrogen-bonded complex that exhibits non-bonding interactions within each benzene ring and a stacking interaction between the benzene rings. We thus have the three main types of interactions: Van der Waals, HB and steric clashes. Whereas van der Waals is well differentiated because it appears at smaller densities, the steric clash and the hydrogen bond spikes overlap in Figure 2.2a. When the Hessian eigenvalues are considered, the different nature of these interactions is made clear: the benzene-ring interactions remain at positive values, whereas the hydrogen bond now lies at negative values, within the attractive regime. The NCI spikes nearest zero density correspond to weakly-attractive dispersion interactions between the phenyl rings.

## 2.2.2

**The 3D plot****2.2.2.1 3D visualization**

The 3D spatial visualisation of the non-covalent interactions as defined above is done using the data from the 2D plots as input to construct 3D plots composed of reduced density gradient isosurfaces.

In a nutshell, a cut-off value of  $s$  close to zero, typically  $s < 0.5$ , is chosen in order to recover all the non-covalent interactions in the system, i.e. all the spikes of the 2D plots. The corresponding reduced density gradient isosurfaces give rise to closed domains in the molecular space which highlight the spatial localization of the interactions within the system (see Figure 2.2c). Since 3D isosurfaces are, by definition, regions of low reduced gradient, the density is nearly constant within these.

At this stage, however, the types of interaction corresponding to the several isosurfaces are not apparent. In order to discriminate between them, the density oriented by the sign of  $\lambda_2$  is further used (as in the 2D plot). A RGB (red-green-blue) coloring scheme is chosen to rank interactions, where red is used for destabilizing interactions, blue for stabilizing interactions and green for delocalized weak interactions. The intensity of these colors (i.e. the deepness of the color) is associated with a higher local density and therefore to a stronger interaction.

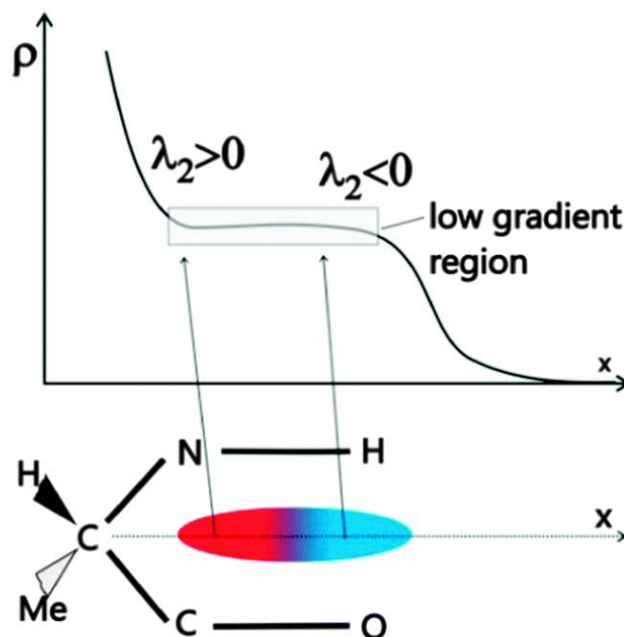
The isovalue (or cut-off) of  $s(\rho)$  chosen for plotting the 3D isosurface determines which features will appear in the NCI plot as well as their spatial extension. On the one hand, all NCI spikes do not strictly achieve  $s=0$ , so that too low a value might miss some of the interactions of interest. [60] On the other hand, too high a value would disclose atomic tails of the density. [61] The cut-off is therefore chosen from the 2D plot so that all spikes, but only spikes, are captured to render a meaningful picture which recovers both attractive and repulsive interactions.

**2.2.2.2 2D and 3D shapes**

Topological features of the electron density are very stable with respect to the calculation method. The main effect of different methods on the  $s$  vs.  $\rho$  diagram is a shift of spikes. The only rule of thumb seems that the same  $s$  value should be used when comparing to each other the various NCI, both in the same or in different systems, provided a single method was employed to obtain the various electron densities. This not being the case, different  $s$  values are seemingly required to compare on similar grounds the  $s$ -based results for differently computed electron density (e.g. from wavefunction, multipolar). In other words, a shift of cut-offs is needed to obtain comparable images. This can be related to the fact that  $s$  roughly behaves like  $\rho^{-1/3}$  (see Eq. 2.3), so that the effect of the method on the density is directly followed by the  $s$ -value. This information is crucial when moving towards bigger systems (see Section 2.3.3).

It emerges that a one-to-one inverse correlation seems to exist among the directionality (and the strength) of specific non-covalent interactions and the surface/volume ratio of the corresponding  $s$  isosurface. In particular, the stronger the interaction, the smaller and more disc-shaped the  $s$  surface appears in real space (and the more negative the  $\rho \times \text{sign}(\lambda_2)$  values are).

In some cases, noticeably in ring closings, bicolored isosurfaces appear (see Figure 2.3). They result from stabilizing features (revealed by the blue color), counterbalanced by destabilising interactions due to steric crowding (revealed by the red color), such as ring closure. [62]



**2.3** Scheme of a mixed color isosurface in a C5 ring formed in the groove between a carbonyl and a NH group within a peptide residue. Within this isosurface, the curvature varies sign, leading to two well differentiated parts. A blue external part which illustrates the directional  $\text{NH} \cdots \text{O}$  interaction and a red part which is indicative of the strain in the 5-membered ring resulting from a multicentric density in the inner region close to the backbone. In the top panel the variation of the density and the sign of  $\lambda_2$  is depicted.

## 2.3

### Learn through examples

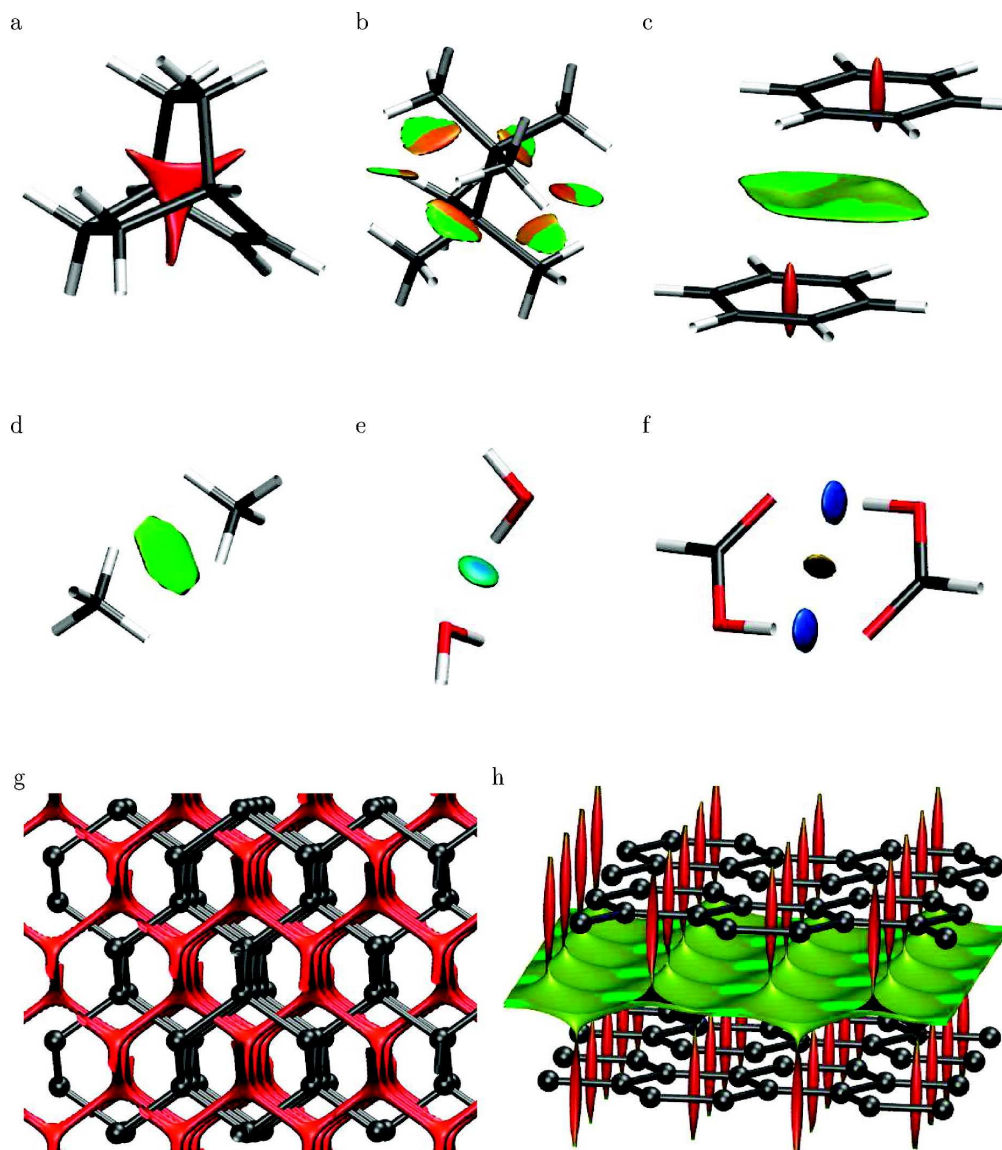
To explore the features associated with small reduced gradients, we will examine 3D NCI plots in representative systems, from small molecules to solids and big systems.

#### 2.3.1

##### Small molecules

Figure 2.4 displays NCI isosurfaces for branched octane, bicyclo[2,2,2]octene, and the homomolecular dimers of methane, benzene, water, and formic acid. These isosurfaces provide a rich visualization of non-covalent interactions as broad areas of real space, rather than simple pair-wise contacts between atoms. We first consider the sterically-crowded molecules bicyclo[2,2,2]octene (Figure 2.4a) and the branched octane isomer (Figure 2.4b). In the first case, the low-density, low-gradient region corresponds to the center of the cage, where steric repulsion between the bridgehead carbons is expected. For the branched octane isomer, the isosurface lies between the closely-interacting methyl groups on opposite sides of the central C-C bond. The interactions are repulsive nearer the C-C bond and weakly attractive between the hydrogen atoms. Dispersion and hydrogen bonding can also be clearly detected. In the dispersion-bound methane dimer (Figure 2.4d), the isosurface forms a disc between the individual monomers. For the water dimer (Figure 2.4e), the isosurface lies between a hydrogen donor and oxygen acceptor, characteristic of hydrogen bonds. The formic acid dimer (Figure 2.4f) reveals stronger HBs than in the water dimer, and also weak van der Waals interactions between the two closely-interacting acidic hydrogens.

Finally, in the benzene dimer (Figure 2.4c), there is an area of non-bonded overlap located at the center of each benzene ring, resembling the isosurface for bicyclo[2,2,2]octene. There is another lower-density surface



**2.4** NCI isosurfaces ( $s = 0.5$ ) for a) branched octane, b) bicyclo[2,2,2]octane, and the homomolecular dimers of c) benzene, d) methane, e) water, and f) formic acid. Gradient isosurfaces are also shown for cuboid sections of g) diamond and h) graphite. Color coding in the range  $-0.04 < \text{sign}(\lambda_2)\rho < +0.02$  au.

between the overlapping portions of the benzenes, where  $\pi$ -stacking is expected. It is important to compare this image to the ones displayed in Table 1.1. The intermolecular interaction in benzene dimer appears very clearly with NCI as a surface that highlights the benzene to benzene stacking interaction, well beyond the pair interactions found with AIM.

### 2.3.2 Solids

As we saw in the Introduction (Section 1.3.1), non-covalent interactions in solid state have raised a great deal of interest lately, due to their relevance for self-assembly [36] and crystallization [37] processes.

Indeed, crystalline solids exhibit rich and challenging bonding patterns. We consider the prototypical examples of carbon in the diamond (Figure 2.4g) and graphite (Figure 2.4h) phases at their equilibrium geometries. In diamond, the carbon atoms are  $sp^3$  hybridized and are connected by strong covalent bonds that form a tridimensional, tetrahedral network. Figure 2.4g shows a NCI isosurface for a cuboid section of the diamond crystal. The non-covalent surface extends through the voids of the structure, creating a network similar to that of the covalent bonds.

Graphite in its  $\alpha$  form (Figure 2.4h) has a bidimensional, hexagonal lattice, with the carbon atoms  $sp^2$  hybridized and covalently bonded to their three nearest neighbors. The NCI isosurface shows areas of nonbonded overlap at the center of the hexagonal rings, as seen previously in benzene.  $\pi - \pi$  stacking interactions between the graphene sheets are clearly manifested by the isosurfaces filling the interlayer spaces.

### 2.3.3

#### Biological Systems

Understanding of non-covalent interactions is crucial for the comprehension of the 3D structure and, thus, of the activity of biosystems. [65, 66] However, the calculation of the electron density in these systems is totally unbearable. Approximations need thus to be sought.

##### 2.3.3.1 Promolecular densities

Densities are stable (see Section 2.2.2.2) to such an extent that NCI characteristics are already contained in the sum of atomic densities,  $\rho_i^{at}$ . [63, 64] The resulting molecular density, also known as promolecular density,  $\rho^{pro}$ , is then given by:

$$\rho^{pro} = \sum_i \rho_i^{at} \quad (2.4)$$

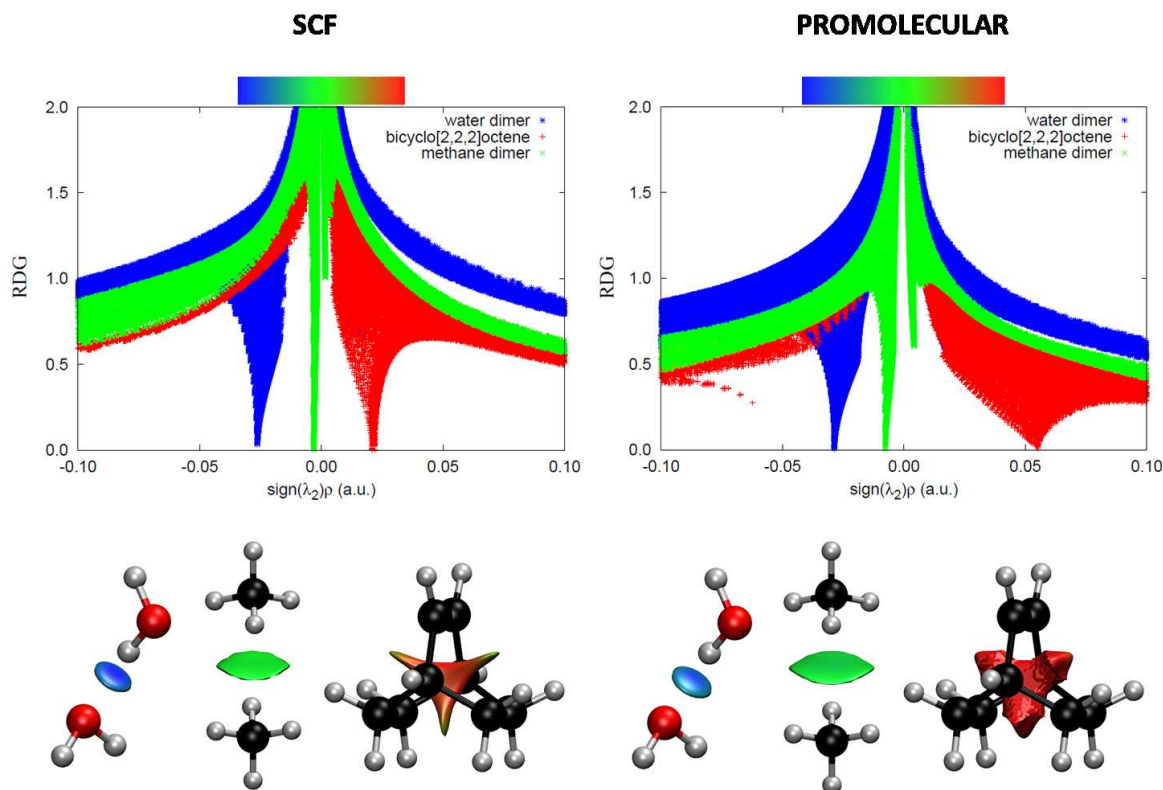
A promolecular density obtained from simple exponential atomic pieces is able to predict low-density, low-reduced-gradient regions similar to density-functional results:

$$\rho_i^{at} = \sum_j c_j e^{-\bar{r}/\eta_j} \quad (2.5)$$

where  $c_j$  and  $\eta_j$  are adjusted to fit closely spherically-averaged, density-functional atomic densities (see Appendix I).

Figure 2.5 shows the  $s^{pro}$  versus  $\rho^{pro}$  for bicyclo[2,2,2]octene, methane dimer and water dimer. It shows the same 2D features seen in Figure 2.1. Also, 3D isosurfaces generated from the promolecular density (Figure 2.5) are very similar to those obtained previously with self-consistent DFT and even MP2 densities (Figure 2.4). For all cases considered, results at the self-consistent and promolecular level are qualitatively equivalent. Only slight quantitative differences are introduced by density relaxation that, as expected, shift the  $s$  versus  $\rho$  spikes to more bonding regimes. Specifically, a large shift toward smaller density values is observed in the spikes corresponding to non-bonded overlap, introducing less repulsion and greater stability. Taking this shift into account in the choice of isosurfaces, results at the self-consistent and promolecular level are qualitatively equivalent for all cases considered (see Figure 2.5 bottom). For example, lower cut-offs on the gradient (0.25-0.35) and higher cut-offs on the density (0.08-0.09 au) were required in order to generate the isosurface for bicyclo[2,2,2]octene.

Promolecular densities obviously lack relaxation; however, the promolecular densities are extremely useful in biomolecular systems, such as proteins or DNA. Because the calculation of the electron density in these systems becomes extremely computationally expensive, the promolecular density becomes an attractive option: non-covalent interactions can be analyzed with only the molecular geometry required as input.



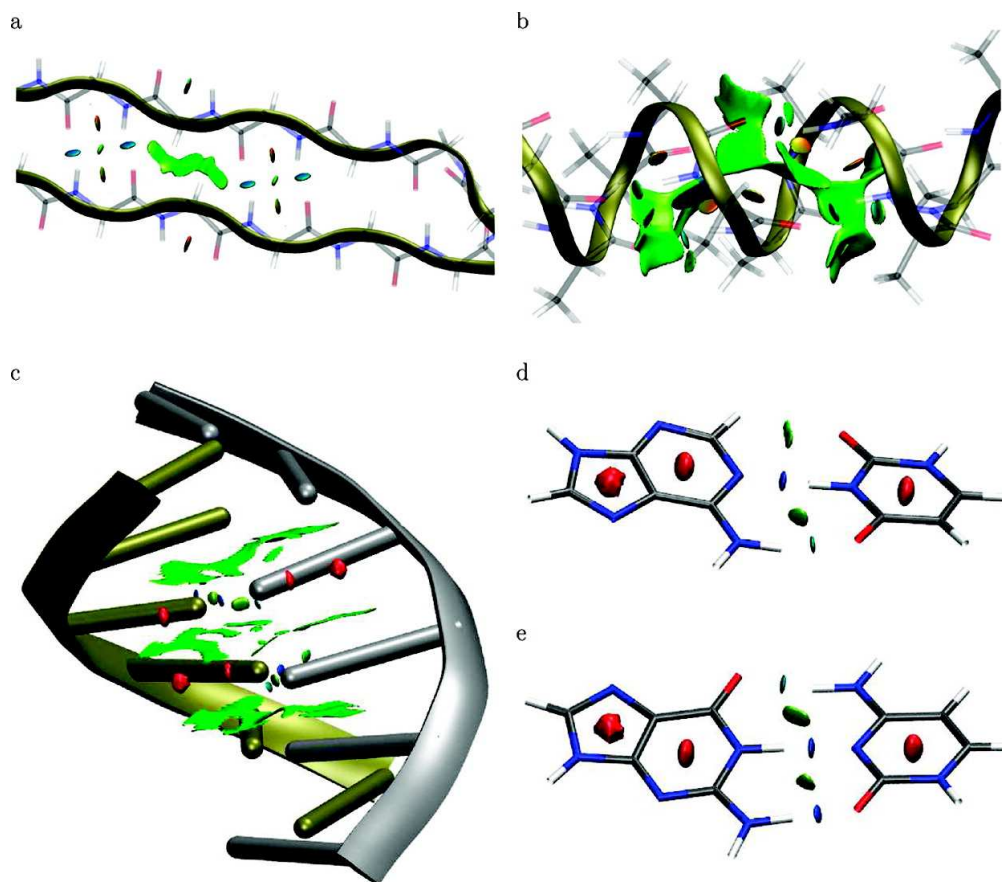
**2.5** Comparison between SCF and promolecular NCI results. The same  $s(\rho)$  features are obtained using self-consistent (left) and promolecular (right) calculations, with a shift toward negative (stabilizing) regimes. Bottom: Taking the shift in spikes into account (i.e., changing the cut-off), the isosurface shapes remain qualitatively unaltered for selected small molecules. Figures are shown for both SCF (left) and promolecular densities (right). NCI surfaces correspond to  $s = 0.6$  and a color scale of  $-0.03 < \rho \text{ sign}(\lambda_2) < +0.03$  au for SCF densities. For promolecular densities,  $s = 0.5$  (water and methane dimers) or  $s = 0.35$  (bicyclo[2,2,2]octene), and the color scale is  $-0.04 < \rho \text{ sign}(\lambda_2) < +0.04$  au.

### 2.3.3.2 Examples

We first consider two model polypeptides: an  $\alpha$ -helix consisting of 15 alanine residues and an anti-parallel  $\beta$ -sheet consisting of 17 glycine residues. Figure 2.6 displays NCI isosurfaces for cuboid regions at the center of these polypeptides. For the  $\beta$ -sheet, the lowest-density portions of the gradient isosurface arise from hydrophobic, dispersion-dominated interactions, primarily involving the  $\text{CH}_2$  groups of the glycines. The higher-density regions correspond to inter-residue hydrogen-bonds and repulsive interactions between the adjacent C=O and N-H groups. For the  $\alpha$ -helix, the isosurface has a large, low-density region within the helix and between the side-chain methyl groups. The higher-density portions of the isosurface correspond to inter-residue hydrogen-bonds along the helix and repulsive interactions between adjacent N-H groups.

We also considered the non-covalent interactions between nucleobases in the B-form of double-strand, six-base-pair (TGTGTG) DNA (Figure 2.6c). The NCI isosurface resembles that of graphite, with broad, low-density regions indicative of  $\pi$ -stacking between base-steps. The interactions between individual deoxyadenosine-deoxythymidine and deoxycytidine-deoxyguanosine pairs are shown in Figure 2.6d,e. The isosurfaces show non-bonded overlap within the nucleobase rings, as in benzene and graphite, and hydrogen-bonding motifs similar to the formic acid dimer. The strong  $\text{N-H} \cdots \text{O}$  and  $\text{N-H} \cdots \text{N}$  hydrogen bonds can be clearly distinguished from the weaker, attractive  $\text{C-H} \cdots \text{O}$  interaction by the density values, as shown in different colors.

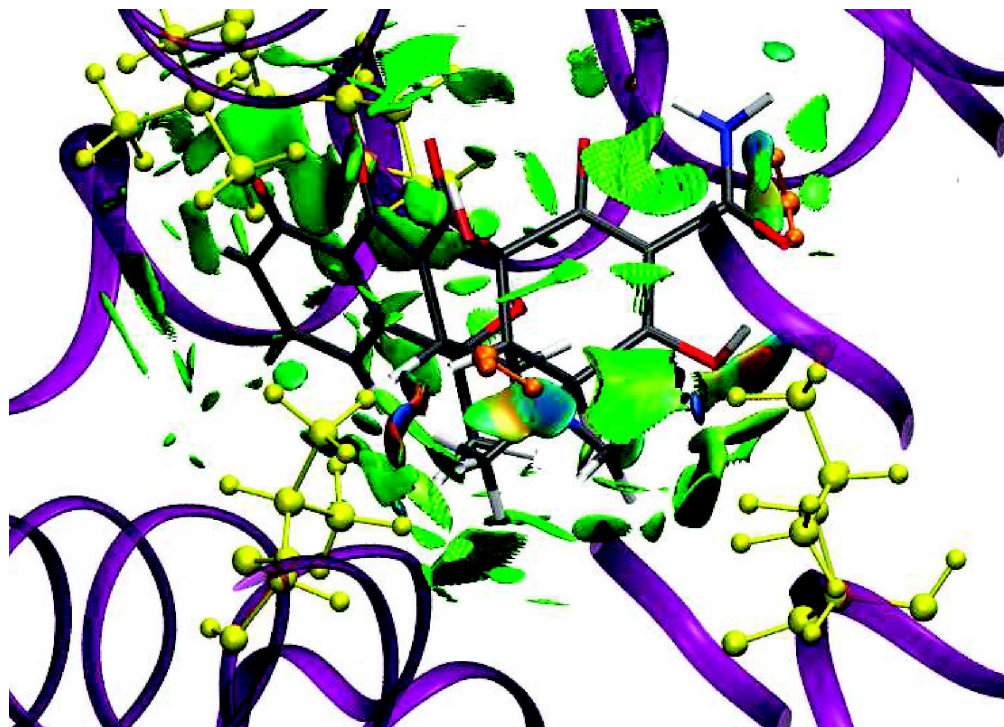




**2.6** Gradient isosurfaces ( $s^{pro} = 0.35$ ) for cuboid sections of the (a)  $\beta$ -sheet and (b)  $\alpha$ -helix polypeptides. Gradient isosurfaces ( $s^{pro} = 0.25$ ) are also shown for the (c) B-form of DNA, and the (d) A-T and (e) C-G base pairs. The surfaces are colored according to values of  $\text{sign}(\lambda_2)\rho$ , ranging from -0.06 to +0.05 au. Geometries of the polypeptides were obtained with the MMFF force field using the spartan program. [67] Both were capped with  $\text{COCH}_3$  and  $\text{NHCH}_3$  groups. The DNA structure was obtained using the X3DNA program [68] with ideal geometry parameters. [69]

The hydrogen-bonding surfaces in the DNA model have density values of ca. 0.065 au, compared to density values of ca. 0.035 au for the polypeptide hydrogen bonds. This is evident from the degree of blue shading for the hydrogen bonds in Figure 2.6. Since density values at hydrogen-bond critical points correlate with the interaction strength, [25,70] NCI results indicate that the hydrogen bonds between nucleobase pairs are substantially stronger than between amino acids, in agreement with literature data. [71–73]

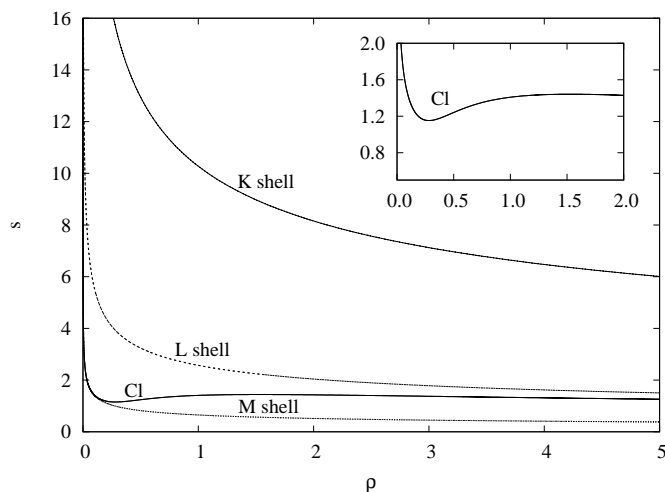
Let us now consider the interaction between a ligand and a protein active site. The low-gradient isosurface for a tetracycline inhibitor bound to the tetR protein in Figure 2.7 shows a complex web of non-covalent interactions between the ligand and active site. When analyzing non-covalent interactions in protein-ligand complexes, it is usually assumed that these interactions are due to a specific contact between two atoms. [44] However, it is clearly seen in Figure 2.7 that this assumption is only partly correct. Hydrogen bonds, such as those between the tetracycline amine groups and two water molecules (shown in orange), are directional and specific. Conversely, van der Waals, dipole-dipole, and hydrophobic interactions, such as those between the tetracycline and the Leu61, Val91, Ile136, and Val166 residues (shown in yellow), are not atom-specific and occupy broader regions in space. The figure reveals some steric clashes (orange and red regions of the isosurface) that must be offset by stronger, attractive interactions to give binding in this crystal structure. A ligand “fits” the geometry of the active site, and the interaction energy between the ligand and protein is



2.7 Gradient isosurfaces ( $s_{pro} = 0.35$ ) for interaction between the tetR protein and tetracycline inhibitor. Surfaces colored in the  $\text{sign}(\lambda_2)\rho$  range from -0.06 to +0.05 au.

comprised of many small contributions. When trying to design a new ligand to fit a specific active site, one should consider all such interactions.





**3.1** Promolecular model for Cl atom. Each shell is represented by an exponential as in Eq. 2.5, yielding 3 shell lines (K,L,M) for chlorine. The slope change observed in the ionic plots is highlighted in the inset. It is due to the fact that those densities are mainly dominated by the L shell and not anymore by the M shell.

### 3 Only weak bonds?

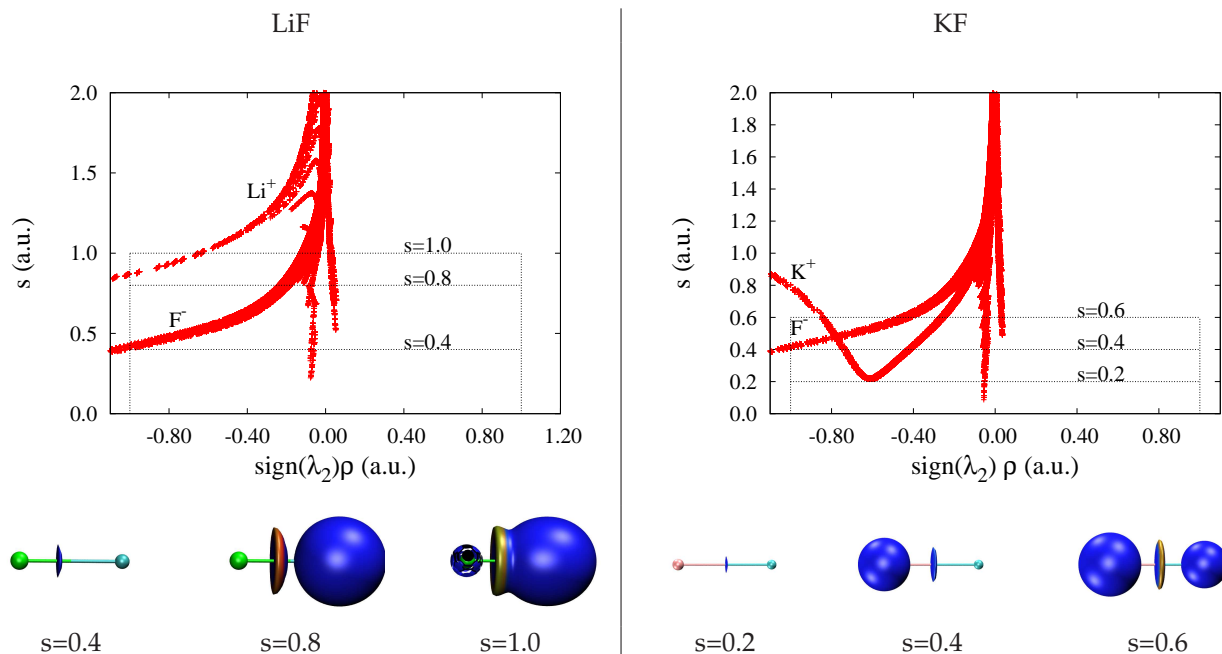
Just as much as the electron density is able to reveal all types of bonds, NCI also is. Moreover, the behavior of  $s(\rho)$  is related to that of  $\nabla\rho/\rho$ , which is known to reveal atomic shells. Thus, although not usually exploited, we should not forget that NCI provides information about all these electronic features.

#### 3.1 Atomic shells

Fig. 3.1 shows the promolecular model for the chlorine density, where several changes in slope are observed. This can be easily analyzed from the model promolecular densities  $\rho(r) \simeq \sum_j \rho_j(r) = \sum_j c_j e^{-d_j r}$ . Thus, each shell gives rise to a  $s(\rho)$  curve of a  $y = cx^{-1/3}$  exponential behavior, where the constant  $c$ , determines the displacement of the curve along the  $y$  axis and is related to the hardness of the shell (see Section 3.2 for a visual example.)

#### 3.2 Ionic bonds

Within non covalent interactions, ionic ones are probably the strongest ones and very relevant for example in binding sites with ions. LiF and KF have been chosen as representative examples of ionic interactions.



**3.2** NCI for LiF (left) and KF (right). Top:  $s(\rho)$ , Bottom: NCI isosurfaces for various cutoffs (indicated below each figure). The part of the  $s(\rho)$  diagram covered by each isosurface is highlighted in the  $s(\rho)$  plot by the corresponding frames.

Densities in ionic crystals are almost non overlapping, thus they are well described by promolecular densities (Section 2.3.3). We approach atomic/ionic densities by exponential basis functions for each shell [63, 64]. In the region of the interaction, this reduces to the valence (i.e. the outermost shell), so that the density for an ionic pair AB at a mutual distance  $R$  is given by:

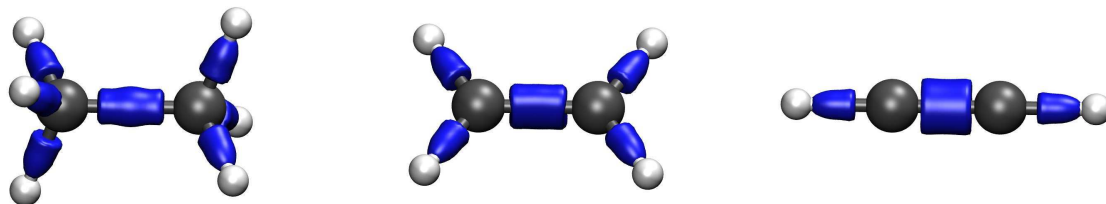
$$\rho(r) = \rho_A^{prom} + \rho_B^{prom} = ae^{-\alpha r} + be^{-\beta(R-r)} \quad (3.1)$$

where  $a$ ,  $\alpha$ ,  $b$  and  $\beta$  are positive constants characteristic of the A and B ions, respectively. [74]

From what we have seen, the exponential constants  $\alpha$  and  $\beta$  are associated with the difficulty to deform, or hardness, of the ions. [74] Thus, the relative position of the curves can be associated with the relative hardness of the ions. Since cations are generally harder than anions, i.e.  $\alpha > \beta$ , in most cases the cation curve will be over the anionic line at low (valence) densities. This is exactly what is observed in LiF in Fig. 3.2 top (results are similar for NaX). Two decaying curves, one for each ion, with the cation on top of the anion by  $\alpha - \beta$ . However, for potassium salts, the cation contribution is softer, yielding even to an inversion for KF (Fig. 3.2 right), where the anionic  $F^-$  curve is over the  $K^+$  line at low densities. Indeed, the similar hardness of  $K^+$  and  $F^-$  was already observed within the AIM [74] and ELF [61] topologies.

This provides us with an easy to visualize way to recognize cation-anion contributions to the  $s(\rho)$  plot as well as to cast the relative hardness of the ions: the greater the difference between the curves, the greater the ionic hardness difference between them. Note that in the case of third row elements (K,Cl) a sudden change in slope is observed at medium densities, as explained in Section 3.1.

As expected from AIM results, NCI features appear at the ionic bond. Disc-shaped isosurfaces appear in between the ions that represent the ionic bond. Thus, NCI is able to reveal all types of non covalent bonds, be them electronic or electrostatic in origin. The size of the isosurfaces will be greater for fluorides than for chlorides, due to the fact that the peaks for the the former have a greater surface than the latter.



**3.3** B3LYP/6-31G\* gradient isosurfaces with  $s = 0.2$  for ethane, ethylene, and acetylene. The surfaces are colored in the range  $-0.5$  to  $0.0$  au.

### 3.3

#### Covalent bonds

As we saw in Fig. 2.1, covalent bonds can be identified by the reduced density gradient as peaks in the  $s(\rho)$  diagram at larger densities. This is possible since covalent bonds show a saddle point in the density, where  $s = 0$ . The low-gradient isosurfaces are also distinctly different for single, double, and triple bonds; results are shown for the ethane, ethylene, acetylene series in Figure 3.3.



## 4 AIM and Beyond

We have seen that there is a coherent description of strong localized attractive non covalent interactions by AIM and NCI. However, this is not always the case. In the coming sections we will describe these discrepancies, which can be classified according to the following scheme:

- Repulsive interactions
- Attractive interactions
  - very weak interactions
  - delocalized interactions
- Absence of interactions

### 4.1

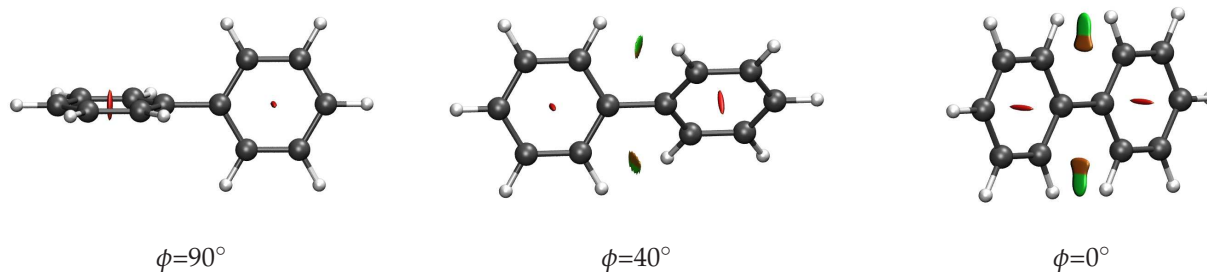
#### Repulsive BCPs?

The most stable structure of biphenyl is twisted ( $\phi=44^\circ$ ). It lies 1.4 kcal/mol lower in energy than the planar geometry ( $\phi=0^\circ$ ) and 1.6 kcal/mol lower in energy than the perpendicular geometry ( $\phi=90^\circ$ ). [75,76] From a chemical point of view, this can be understood as an equilibrium between aromaticity and steric repulsion. Whereas the perpendicular geometry breaks the delocalization of the  $\pi$  density over the two rings, the planar structure is subject to steric non-bonded repulsion between adjacent atoms of the bridge. These two factors roughly balance, giving rise to stabilization of the twisted structure.

This has caused much controversy within the classical AIM approach. [75,76] In spite of showing a bond point between the ortho hydrogens, the parallel structure is not favored. On the one hand, Bickelhaupt et al. believe that the bond point in between hydrogens should be associated with steric repulsion instead of a bonding interaction. [75] Bader and coworkers, instead, think that the H-H contribution to energy is stabilizing, whereas the destabilization comes from elongation of the bridging C-C bond. [76]

The picture provided by NCI is able to reconcile both points of view. Figure 4.1 shows the NCI surfaces for orthogonal, twisted, and parallel biphenyl geometries. It can be seen that the absence of non-covalent interactions in the orthogonal arrangement (Figure 4.1a) is in agreement with it being the highest-energy conformer. The parallel conformer, instead, shows both stabilizing H-H interactions as well as strong steric clashes (Figure 4.1c). These do not arise from the H-H direction, which is indeed an accumulation of density, but from the whole non bonding region, where H-C-C-H densities overlap. This destabilizing interaction can be softened by slightly twisting the benzene rings. At  $40^\circ$  both interactions diminish, giving rise to the balance that characterizes the stable conformation (Figure 4.1b). Thus, the H-H interaction alone is indeed slightly stabilizing, but a greater steric repulsion arises in the area due to the non-bonded overlap of densities. This is actually reflected in the increase of the C-C bonding distance from 2.808 bohr in the stable structure to 2.824 bohr in the parallel structure.





4.1 Biphenyl NCI surfaces at  $90^\circ$ ,  $40^\circ$  and  $0^\circ$ .

## 4.2

### Attractive interactions

#### 4.2.1

##### Very weak interactions: missing BCPs?

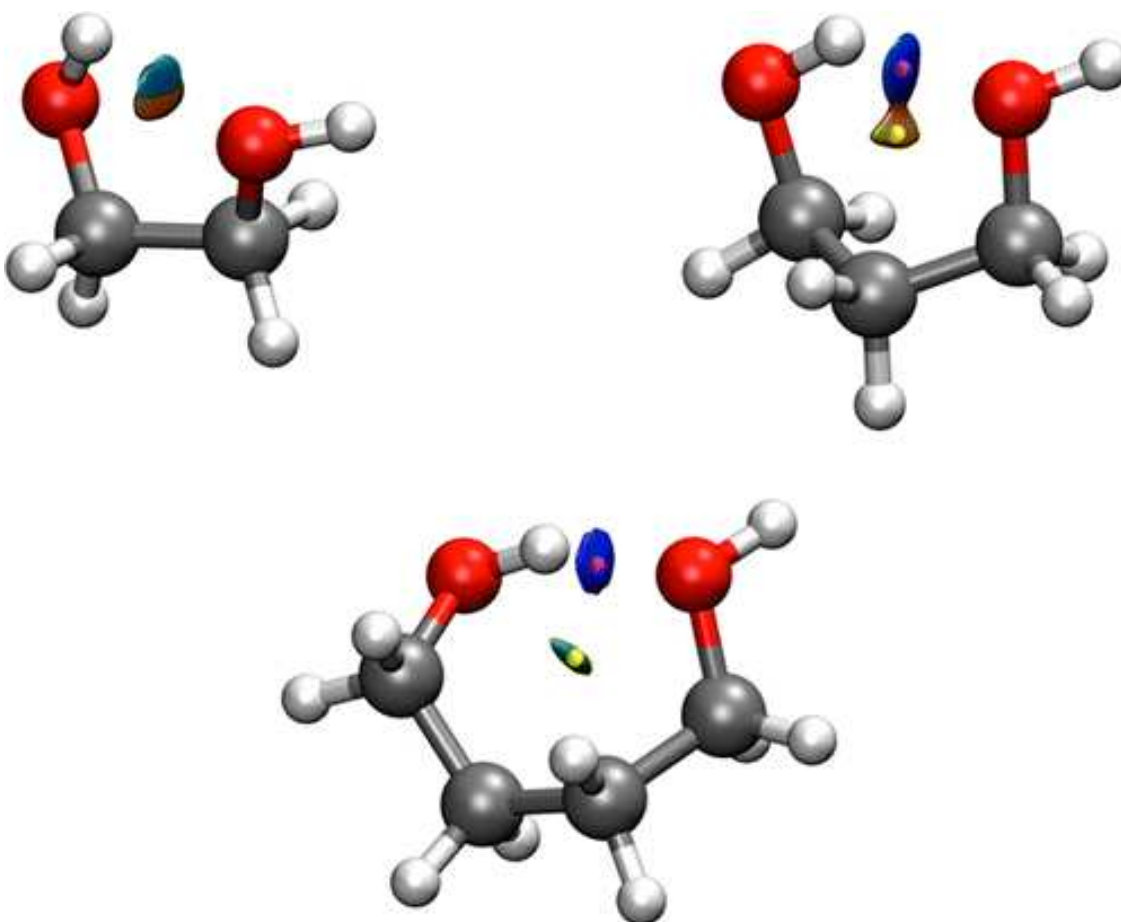
The precise definition of what specifically constitutes a hydrogen bond arouses passionate discourse amongst even the most mild-mannered chemist. AIM theory is routinely used to assess hydrogen bond formation, however its stringent criteria controversially exclude some systems that otherwise appear to exhibit weak hydrogen bonds. As an example, we have analyzed a series of  $1,n$ -alkanediol, which all demonstrate experimental evidence of hydrogen bonding. [78,79]

In Figure 4.2, we present NCI isosurfaces for 1,2-ethanediol (ED), 1,3-propanediol (PD) and 1,4-butanediol (BD) to illustrate the nature of the intramolecular hydrogen bonding interactions. Also included in Figure 4.2 are the corresponding BCPs (small yellow spheres) and RCPs (small red spheres) that highlight the complementarity of the AIM and NCI approaches.

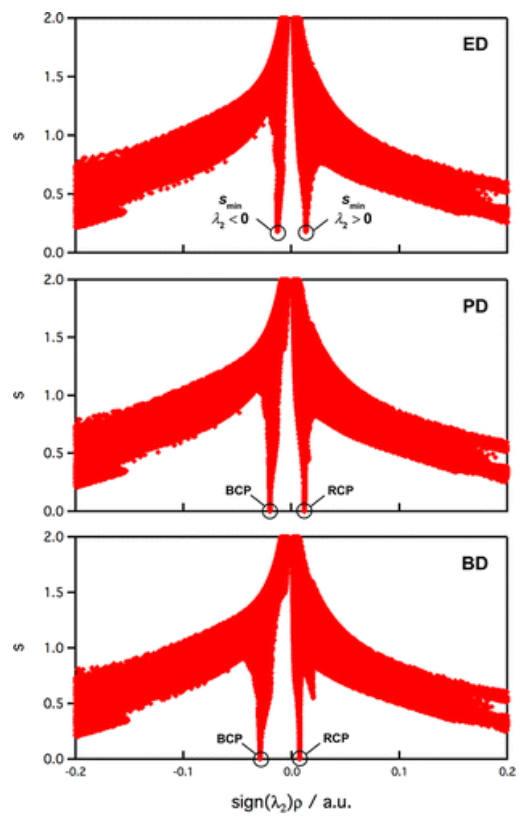
For BD and PD the BCPs clearly appear between the hydroxyl groups and are accompanied by ring critical points (RCPs) towards the center of the ring. For ED, the two types of critical points collapse onto each other. Consequently, only PD and BD satisfy the AIM criteria for hydrogen bonding, but not ED. This is despite the fact that all three molecules demonstrate experimental evidence of hydrogen bonding.

The image of BD corresponds to a typical strong hydrogen bond within the NCI framework. Blue in color and very disk-shaped, that is, a very localized interaction, which expands from the BCP (see Section 2.2.2). A second weaker interaction is evident from the green isosurface at the center of the ring, which is related to the RCP. For PD, at the same isosurface value both interactions start to mix. However, the presence of critical points is still clearly marked by a distinct blue region centered at the BCP corresponding to a moderate hydrogen bond and a distinct green region centered at the RCP. Finally, the absence of critical points in ED is reflected as a unique NCI isosurface for the same  $s$  value. This isosurface is a single circular volume, which is polarized blue-green between the two OH moieties due to collapse of both regions of interaction in the intramolecular bonding.

Where is this discrepancy coming from? In Figure 4.3, we present 2D NCI plots. In all three molecules two spikes are obtained for the interaction, with one spike at negative  $\lambda_2$  corresponding to an attractive hydrogen bonding interaction and a second spike at positive  $\lambda_2$  corresponding to a repulsive steric interaction due to ring formation. The only difference arises in the minimum values of  $s$  attained in the graphs: whereas BD and PD attain zero (as expected from the presence of critical points), ED does not. However, it does present the same  $s(\rho)$  pattern. In summary, we find there to be no clear distinction between the nature of the intramolecular hydrogen bonding interactions in ED, PD, and BD, despite the absence of a BCP in ED. AIM is too constraining for very weak interactions, which NCI has no difficulties in identifying.



**4.2** NCI isosurfaces for ED (top left), PD (top right), and BD (bottom):  $s = 0.5$  and a blue-green-red color scale from  $-0.03 < \text{sign}(\lambda_2)\rho < +0.03$  au. Small spheres represent critical points: BCPs in green and RCPs in red. Optimizations were carried out with the explicitly correlated coupled cluster singles, doubles and perturbative triples [CCSD(T)-F12a] method as implemented in MOLPRO 2010.1. [80] A continuous change is observed in the isosurfaces from ED to BD.



4.3 Plot of the reduced density gradient  $s$  and  $\text{sign}(\lambda_2)\rho$  for ED (top), PD (middle), and BD (bottom). The density features are qualitatively the same with a continuous change observed from ED to BD.

## 4.2.2

**Delocalized interactions: which BCP?**

Dispersion interactions are due to time-dependent perturbations of the electron density and imply correlations among distant electrons. Therefore, they cannot be correctly taken into account by ground state adiabatic methods, such as standard DFT theory, where the exchange-correlation potential is estimated on the basis of a finite number of the static electron density derivatives. [93, 94] Moreover, dispersion interactions are inherently non-local in nature, as they correlate the overall charge density distributions of individual molecular moieties to each other. On the other hand, it is also known that dispersion forces do not significantly affect electron density, although they play an important role in lowering the overall interaction energy of the system. [95] We should not forget that for these interactions, the density changes are so small that MP2/6-311++G\*\* calculations produce virtually identical NCI isosurfaces as the B3LYP/6-31G\* ones, despite the different interaction energy estimates of these two methods.

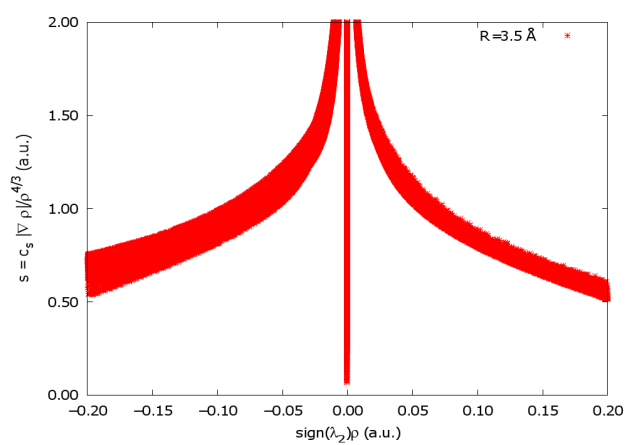
The electronic excitations causing dispersive interactions are clearly always present, but the characteristic large and flat NCI isosurfaces associated to such interactions emerge only if stronger interactions (such as, for example, OH...O hydrogen bonds) are not simultaneously acting within the same region of space. Moreover, strictly speaking, purely dispersive, van der Waals interactions are always attractive. In van der Waals NCI pictures, however, the  $\text{sign}(\lambda_2)$  quantity can be positive or negative throughout the NCI isosurface. This does not indicate that atoms are in “nonbonded” contact (closed-shell interactions), not that the overall interaction revealed by the NCI isosurface is destabilizing. One should always remember that NCI explores the behavior of  $s$  in a specific region, whereas the interaction energy is the result of a balance involving forces which effectively operate in a larger portion of space. A given conformation is the outcome of a subtle competition among different energy contributions, and there is always a certain degree of arbitrariness in partitioning the overall cohesive energy of a crystal in stabilizing and repulsive terms. As reminded by Bader, [24, 96, 97] there are no net attractive or repulsive forces acting on a field-free quantum system at the equilibrium, as in that case the overall balance of the quantum-mechanical Eherenfest and Feynman forces (acting respectively on electrons and nuclei) is exactly zero. In conclusion, the so-called van der Waals-like large and flat NCI isosurfaces above described should be considered as tools to highlight those regions of space characterized by steric crowding and dispersive interaction balance, rather than as a way to “see” or “localize” van der Waals, dispersive interactions, which by their very nature are neither local nor static. This said, we should not forget that NCI is able to reveal the molecular nature of van der Waals (not 2-center).

## 4.3

**Absence of interaction: too many BCPs**

One of the problems of associating interactions with critical points is that some critical points are imposed by symmetry constraints, beyond their physico-chemical meaning. The most common example of such case is the stretching of a molecule to infinity. Even though at very large distances molecules will not interact with one another, symmetry imposes the appearance of at least one critical point between them. The use of surfaces and volumes instead of critical points to identify interactions naturally overcomes this limitation.

Figure 4.4 shows  $s(\rho)$  diagrams and NCI isosurfaces for the water dimer at very long separations ( $d = 3.5 \text{ \AA}$ ). At this distance, the NCI region reduces to the BCP: the  $s(\rho)$  peak is extremely sharp, such that the NCI surface and critical point basically coincide. The stabilization of the complex does not extend to other regions of space beyond the critical point itself. As we will see in Chapter 6, the volume of the NCI region can be associated with the degree of stabilization. Thus, at infinite separation, NCI is able to supersede symmetry constraints that compel the appearance of a critical point and identify that the monomers are not interacting at infinite separation.



4.4 a)  $s(\rho)$  diagrams and b) NCI isosurface in the non interacting regime ( $d = 3.5\text{\AA}$ ). The isosurface was generated for  $s = 0.6$  au and  $-0.04 < \text{sign}(\lambda_2)\rho < 0.04$  au.

## 5 Software

In this chapter, we introduce the computational algorithms and their practical implementation for the analysis and visualization of weak interactions by means of NCI. We review the implementation for both self-consistent fully quantum-chemical, promolecular and experimental densities in molecules and solids.

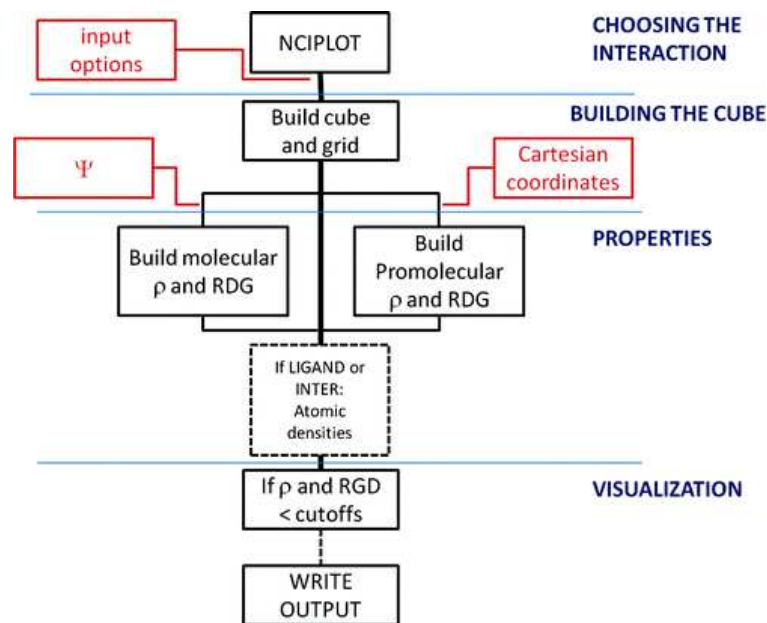
### 5.1 Molecules

Molecular NCI features are implemented in the code NCIPLLOT, whose algorithmic details are reviewed below.

#### 5.1.1 Algorithmic details

Figure 5.1 shows a simplified flow diagram for the visualization on non-covalent interactions in NCIPLLOT. Summary details of the tasks completed by each routine along each of the steps underlined in the flowchart are shown in Table 5.2 (cube construction, properties, visualization, and I/O flow).

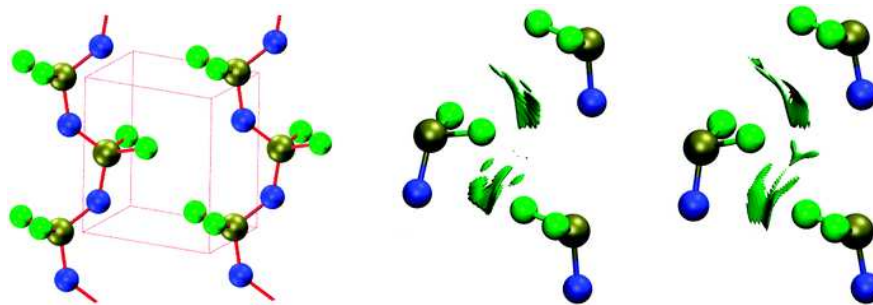
Two basic processes have been highlighted in Fig. 5.1. The input of data is shown in red, whereas their internal treatment is summarized in black. Two basic types of data constitute the input: the density information (wavefunction or molecular geometry) and the treatment options, which will determine the non-covalent interactions to be plotted. The internal algorithms to which the data are subjected can be divided in four main blocks: (i) the selective choice of interactions (through the input), (ii) the construction of the cube and the grid (carried at CUBE, see table 5.2), (iii) the construction of properties at each point (which utilizes a number of routines), and (iv) the construction of visualization data (carried by the main routine, NCIPLLOT). Since the input is keyword oriented, the program also includes a number of parsing routines.



5.1 Flow diagram of the organization of the program routines for visualization of non covalent interactions in NCIPLLOT. Red labels highlight the information that is/might be input by the user, whereas black labels show the internal flow of information. Flow has been divided into the four main algorithmic parts of the program: input, cube construction, properties, and visualization.

5.2 Tasks completed by NCIPLLOT and details of the Input and Output. The table has been organized following the main algorithmic subdivisions of the flowchart (Figure 5.1): cube construction, properties, and visualization, as well as I/O flow.

MODULE	TASK	INPUT	OUTPUT
<b>visualization</b>			
NCIPLLOT	main routine	-----	visualization
<b>cube and grid</b>			
CUBE	constructs cube and grid	geometry	cube, grid
<b>I/O routines</b>			
TIMER	accumulates running times	process and resetting	elapsed times
GETARGS	get command	arguments	argument count
GETDATE	extracts time and date	(operating system)	date and time
ZATGUESS	provides atomic #	atomic symbol	atomic #
RWFN	stores wfn information	wfn file	wfn information
RPROM	stores XYZ information	XYZ file	XYZ information
<b>properties</b>			
PROPPROM	calculates properties at $\vec{r}$ (PROM)	$\vec{r}$	$\rho, s$
CALCHESS	calculates $\lambda_2$ at $\vec{r}$ (PROM)	$\vec{r}$	$\lambda_2$
PROPWFN	calculates properties at $\vec{r}$ (SCF)	$\vec{r}$	$\rho, s, \lambda_2$
F012	derivatives at $\vec{r}$ (SCF)	$\vec{r}$	derivatives
PHI012	summation over primitives	$\vec{r}$	summation
PRI012	construction of primitives	$\vec{r}$	primitives
INDEX0	angular momentum assignation	primitive type	$L_i$
RS	matrix diagonalization (eispack)	matrix	eigenvalues



**5.3** The phosphazene polymer poly-NPF<sub>2</sub>, calculated at the experimental geometry [114] (left). The NCI plots have been obtained using the PSPW approach (abinit code, [101, 102] middle) and the FPLAPW method (WIEN2k, [105, 106] right).

## 5.2

### Solids

#### 5.2.1

##### NCI for solid wavefunctions

The analysis of NCI for solid-state wavefunctions is carried out using the a code called CRITIC. [98] This program can treat plane-wave, linearized augmented plane-wave, or local exponential basis sets, as opposed to the molecular implementation which only considers Gaussian basis sets (Section 5.1).

##### 5.2.1.1 Algorithmic details

The CRITIC code [99] is interfaced to most common solid-state codes. It can use density information from Quantum ESPRESSO, [100] abinit, [101, 102] VASP, [103, 104] WIEN2k, [105, 106] elk [107] or pi7 [108] as input. In addition, CRITIC reads density cubes in Gaussian [109] and XCrysden [110] formats, so any program not directly supported can be interfaced with CRITIC2 via (relatively sparse) density grids.

In the practical, computational procedure an analytical or grid-based representation of the self-consistent electron density is obtained from a quantum-mechanical calculation or built from a superposition of atomic densities. A parallelepiped spanning the region of interest is chosen and a regular grid is built to encompass it. Depending on the input type, NCI quantities are calculated either analytically or numerically at each grid point.

It is possible to restrict the number of grid points in a variety of convenient ways. In particular, in a PSPW code the density is represented as a uniform grid of values of  $\rho$  spanning the periodic cell. This may be transformed to the corresponding  $\rho_G$  using an efficient three-dimensional Fast Fourier Transform (FFT). This possibility is useful in the computation of the density derivatives that are required to build  $s$  and  $\lambda_2$  because of the simple relationship between the density reciprocal-space coefficients and those of its derivatives. The coefficients of the density gradient and Hessian are transformed back into real-space, and then used to calculate the reduced density gradient and the Hessian eigenvalues. FFT is typically much more efficient than the simple loop over grid points, but the resulting grid necessarily extends over the complete unit cell and the density of the grid may be too low for an adequate representation. To overcome this limitation, a three-dimensional spline interpolation scheme [101, 102] is used to calculate grids denser and in localized regions of space. The use of very dense grids at DFT level is commonplace in the analysis of PSPW results in QTAIM, [111–113] and in our implementation it is avoided by using three-dimensional interpolation.



### 5.2.1.2 Pseudopotentials

In order to assess the validity of the NCI plots obtained with interpolated PSPW densities, Figure 5.3 compares NCI 3D plots obtained from an all-electron full-potential LAPW calculation with the PSPW results for the poly-NPF<sub>2</sub> phosphazene.

Polyphosphazenes are the largest class of inorganic polymers, with high fundamental and technological relevance (see Ref. [115] for a review). Poly-NPF<sub>2</sub> is the simplest member in the family, and the only for which the crystal structure is partially known. [114] In Figure 5.3, the interaction regions of poly-NPF<sub>2</sub> are shown. The PSPW domains are for practical purposes indistinguishable to those obtained using the all-electron method, while the generation of the grid scalar fields for the latter is approximately 30 times slower (of course, the electronic relaxation is also faster in PSPW than in LAPW). The plots show a very weak and localized fluorine-fluorine interaction, similar to stronger halogen bonds, [116] and an only slightly stronger, electrostatic interaction between fluorine and the N-P bond in the neighboring chain, which explains the difficulty in the crystallization of these polymers.

Because of the pseudopotentials, PSPW calculations only work with valence densities, which are smoother but also unphysical in the core regions. It is possible to reconstruct the all-electron density using the (frozen) core orbitals. [118] However, NCI plots are interesting only in valence regions so we take the simple approach of adding a core density that accounts for the missing electrons. This procedure is similar to the construction of the promolecular densities and, in the practical implementation, the two tasks are bundled together. Atomic radial density grids from spherical atomic DFT calculations are used for all atoms in the periodic table. These distance interpolation tables contain the density contribution of all the atomic orbitals in the neutral configuration of the atom. If the promolecular density is needed, it is computed by summing over all orbitals. If only the core density is required, then the sum extends only up to the given number of electrons. This scheme retains the simplicity characteristic of the molecular NCI code.

An important function of the new code is convenient visualization of the NCI regions. The representation of the whole unit cell is seldom informative because the interaction regions are usually straddled across the cell boundary. Also, entire molecules are frequently not contained in the interior of the cell for the conventional origin choice. To successfully present the NCI domains, several interacting molecules must be isolated and only the NCI regions associated with those molecules must be represented. This is achieved by suitably shrinking the representation grids and by considering only the grid nodes for which

1. more than a fraction  $f_{max}$  ( $\approx 0.95$ ) of the promolecular density comes from the selected fragments
2. the contribution of each fragment is less than a certain fraction  $f_{min}$  ( $\approx 0.75$ ) of the total density.

Figure 5.3 for solid calculations exemplifies the use of this technique.

## 5.2.2

### NCI for experimental densities

The NCI index relies exclusively on the electron density and its derivatives, so its implementation in solids also opens interesting new perspectives for the analysis of X-ray experimental densities. [119–121] We have implemented NCI for electron densities derived from single-crystal X-ray diffraction data. Our electron densities were obtained by accurate single-crystal X-ray diffraction experiments at  $T \leq 100$  K.

#### 5.2.2.1 Algorithmic details

Multipole-derived charge densities are known to be possibly biased because of the arbitrariness inherent to the multipolar refinement step. [122, 123]

In the X-Ray implementation NCI is separately applied to molecular pairs extracted from the crystal. This strategy implies that the contribution due to the multipoles centred on atoms belonging to the rest of the unit cell is ignored in reconstructing the multipolar electron density within each pair. In the Hansen-Coppens formalism [124] implemented in the XD program package, [125] the electron density at each point  $\vec{r}$  can,

therefore, be partitioned as follows:

$$\rho(\vec{r}) = \rho_A(\vec{r}) + \Delta\rho(\vec{r}) \quad (5.1)$$

where  $\rho_A(\vec{r})$  is the contribution of a certain (group of) atom(s) or molecule(s)  $A$  and  $\Delta\rho(\vec{r})$  is that arising from the multipoles centred on the remaining atoms in the unit cell.

In general, as the radial part of the multipole functions decays exponentially with  $|\vec{r}|$ , [124] the direct contribution of an atom  $M$ , located at  $\vec{r}_M$ , to the electron density at  $\vec{r}$  is negligible whenever the  $|\vec{r} - \vec{r}_M|$  distance is significantly greater than the covalent radius of  $M$ . Accordingly, the main features of electron density in the space between a pair of nearest neighbour molecules depend almost exclusively on their (composing) pseudoatoms.

Along our tests, we found that this condition was always satisfied, the only exception being that of a single benzene molecular pair. Therefore, NCI can in general be safely performed on a molecular pair extracted from the crystal, the effect of the crystalline matrix being properly and indirectly included in the multipolar expansion of the molecular pair pseudoatoms. It is interesting to note that this approach opens the door to applications of NCI to high accuracy protein data.



## 6 Energy and NCI

Potential-energy curves and the stability of conformers result from interplay of attractive and repulsive contributions, which should ultimately originate from changes in the electron density. [49] However, quantitatively tracing the binding energy back to the density changes in real space is still an unsolved issue. Given that NCI is able to characterize both favorable and unfavorable interactions in real space, it exhibits all the ingredients needed to identify the changes in electron density which give rise to molecular stabilization. Moreover, the ability of NCI to associate real-space regions with non-covalent interactions enables analysis of global properties within these regions, which are subject to change in a quantifiable manner upon stretching.

Along this chapter, we will try to track down the connection between interacting regions and energetics of binding energy curves in hydrogen dimers and in dispersion-based dimer conformations.

### 6.1

#### Integration over NCI regions

In order to quantify the attractive and repulsive contributions to binding, it is necessary to associate a number to the attractive and repulsive NCI volumes, i.e. to integrate them. In order to perform such integrations, it is necessary to establish a unique definition of the NCI region.

Since the difference between the interacting and non-interacting monomers is directly reflected in the  $s(\rho)$  diagram, it is possible to define the NCI region as the points in 3D space with  $(\rho, s)$  values lying in the  $s(\rho)$  peak. To identify this region, both the monomer and the dimer densities must be computed and compared. The lower edge of the monomer  $s(\rho)$  curve is splined (Fig. 6.1a) and all points of the dimer  $s(\rho)$  plot lying below the splined curve are localized in real space (Fig. 6.1a).

Density properties can be integrated within this space to obtain the volume ( $V$ ) of the NCI region, or the charge ( $q$ ) enclosed within it.

$$V_{NCI} = \int_{\Omega_{NCI}} d\vec{r} \quad (6.1)$$

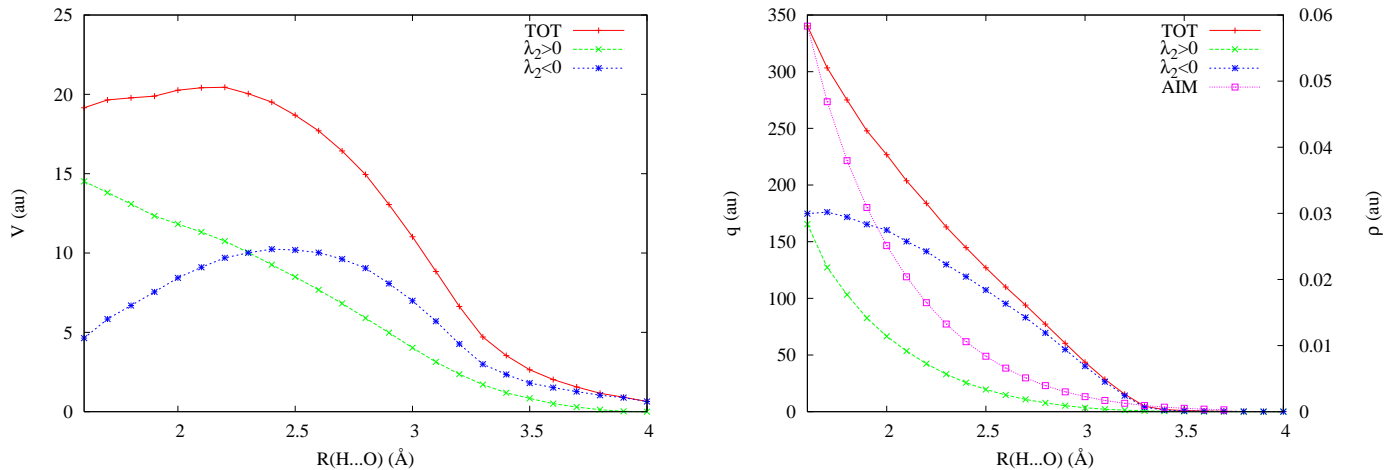
$$q_{NCI} = \int_{\Omega_{NCI}} \rho(\vec{r}) d\vec{r} \quad (6.2)$$

A new version of the program which will be soon released (NCIPLOT-4.0) was developed to perform the volume and charge integrations. It computes pseudo-densities for each of the monomers and splines the resulting  $s(\rho)$  curve. The resulting line is used as a reference in order to identify which  $s(\rho)$  points are only present in the dimer. Integrations are performed numerically, by summation over a cubic grid.

### 6.2

#### Hydrogen bonds binding energy curves

Fig. 6.1a shows the volume of the water dimer NCI region as a function of intermonomer separation. As expected, the volume of the interacting region is negligible at very long distances. As the monomers come closer together, the volume starts to increase, with the volume of the attractive region growing faster than



**6.1** Volume (left) and charge (right) integrations within the hydrogen bond NCI region of water dimer, separated into attractive ( $\lambda_2 < 0$ ) and repulsive ( $\lambda_2 > 0$ ) contributions. The density at the BCP has been included for comparison in the charge integration plot (right).

the repulsive one. At around  $R_{O-H} = 2.5 \text{ \AA}$  the volume of the attractive region becomes nearly constant, and changes in the repulsive region (around the attractive one) become dominant. Eventually, the attractive volume begins to decrease and becomes negligible at very short distances. This result again highlights the necessity of considering the entire non-covalent interaction region rather than just the critical point to understand the corresponding energetics.

When the density of the NCI region is taken into account, Fig. 6.1b is obtained. Although the same overall behavior as Fig. 6.1a is maintained, the shape of the curves change due to the fact that the density in the intermolecular region increases upon dimer compression. The attractive contribution increases more notably at shorter distances, whereas the repulsive part, where the overlap is smaller, increases more slowly. Results for the density at the critical point have been included for comparison. Although  $\rho(\vec{r}_{BCP})$  must increase upon compression due to symmetry constraints, the density associated with the NCI region does not increase continuously, but decreases at short range due to the repulsive wall.

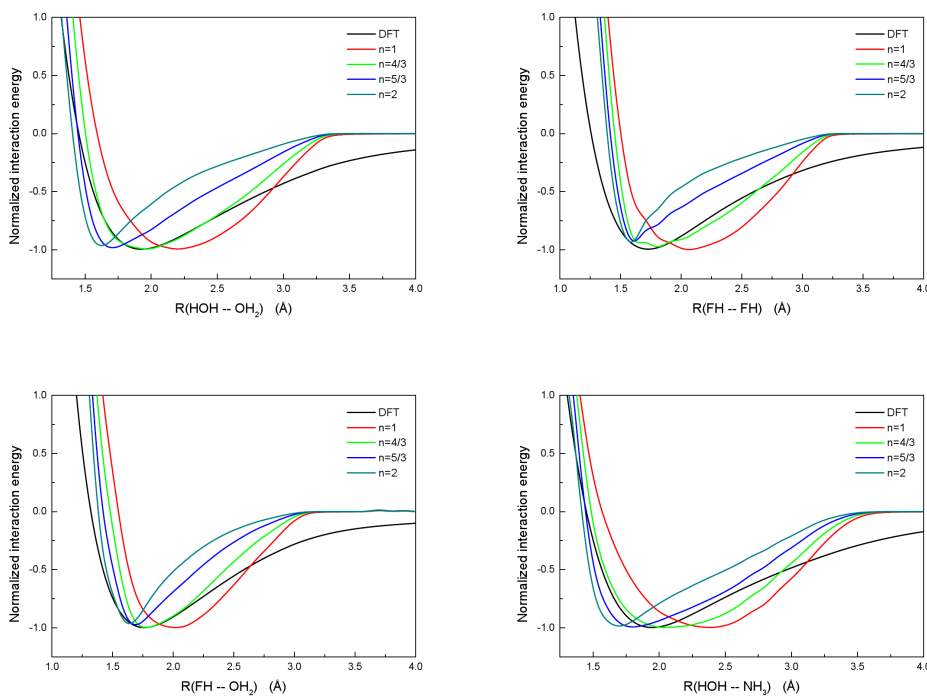
Just as we did in Fig. 6.1, we can separate the attractive and repulsive contributions depending on the sign of the second eigenvalue at each point:

$$q_{att}^n = \int_{\Omega(NCI)} \rho^n(\vec{r}) d\vec{r} \quad | \quad \lambda_2(\vec{r}) < 0 \quad (6.3)$$

$$q_{rep}^n = \int_{\Omega(NCI)} \rho^n(\vec{r}) d\vec{r} \quad | \quad \lambda_2(\vec{r}) > 0 \quad (6.4)$$

$$q_{bind}^n = -(q_{att} - q_{rep}), \quad (6.5)$$

Different exponents,  $n$ , have been considered in order to find the relationship that best fits known binding-energy behavior. Fig. 6.2 shows the results for four conventional hydrogen bonds:  $\text{H}_2\text{O} \cdots \text{H}_2\text{O}$ ,  $\text{HF} \cdots \text{HF}$ ,  $\text{H}_2\text{O} \cdots \text{HF}$  and  $\text{H}_2\text{O} \cdots \text{NH}_3$ . Exponents were chosen in the range of dependencies of the potential-energy and kinetic-energy densities on  $\rho$  ( $\rho^{4/3}$  and  $\rho^{5/3}$ , respectively). The difference between both charge contributions,  $-(q_{att}^n - q_{rep}^n)$ , is able to mimic very reliably the binding energy curves. The best fits are obtained for  $n \in [4/3 - 5/3]$ . For these exponents, the positions of the minima (one of the main characteristics of interatomic potentials) are recovered and the shapes of the curves mimic very well the shapes of the reference binding curves.



**6.2** Binding energies and  $q_{bind}^n$  (Eq. 6.5) for  $\text{H}_2\text{O} \cdots \text{H}_2\text{O}$ ,  $\text{HF} \cdots \text{HF}$ ,  $\text{H}_2\text{O} \cdots \text{HF}$  and  $\text{H}_2\text{O} \cdots \text{NH}_3$ . Results for several exponents ( $n = 1, \frac{4}{3}, \frac{5}{3}$  and 2) are collected for comparison. All the curves are normalized to minimum values of -1.

## 6.3

### Dispersion and additivity

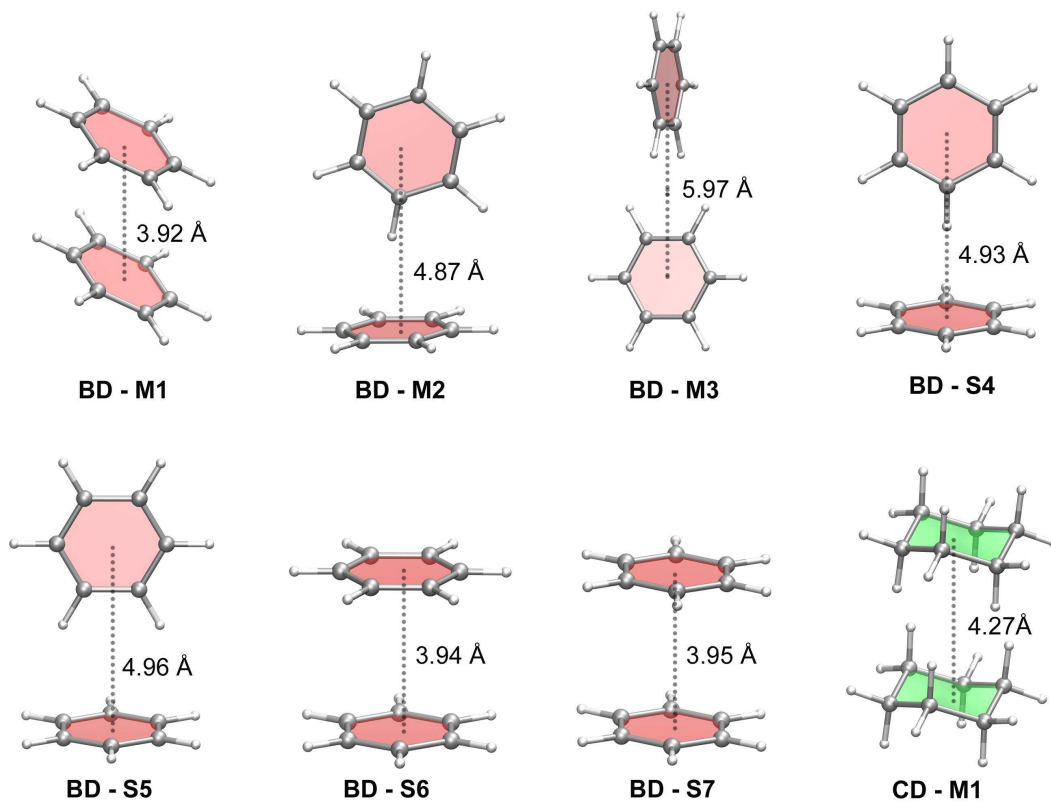
Among non covalent interactions, those involving aromatic rings, [126] such as  $\pi - \pi$  stacking, ion- $\pi$  and CH- $\pi$  interactions are especially relevant due to their importance in many applications. [127–133] Nevertheless, although the term “aromatic interactions” is widely used to describe these interactions, monomer aromaticity was recently proven not to be a mandatory feature for stacking interactions. [24, 134] In fact, cyclohexane and benzene show similar melting and boiling points, indicating that  $\pi - \pi$  and  $\sigma - \sigma$  interactions are essentially equal. [133] Therefore, a crucial question appears as to the reason behind  $\pi - \pi$  being an ever-present pattern, whereas  $\sigma - \sigma$  are not. Thus, discerning between  $\pi - \pi$  and  $\sigma - \sigma$  interactions, their origin and their energetics constitutes a perfect problem to understand the relationship between NCI and dispersion energetics.

Based on previous investigations, [135, 136] we have considered seven conformations of benzene dimer (BD) as well as one for cyclohexane dimer (CD) (see Figure 6.3). The additional label M/S indicates minimum/saddle-point conformations.

#### 6.3.1

##### The origin of stabilization

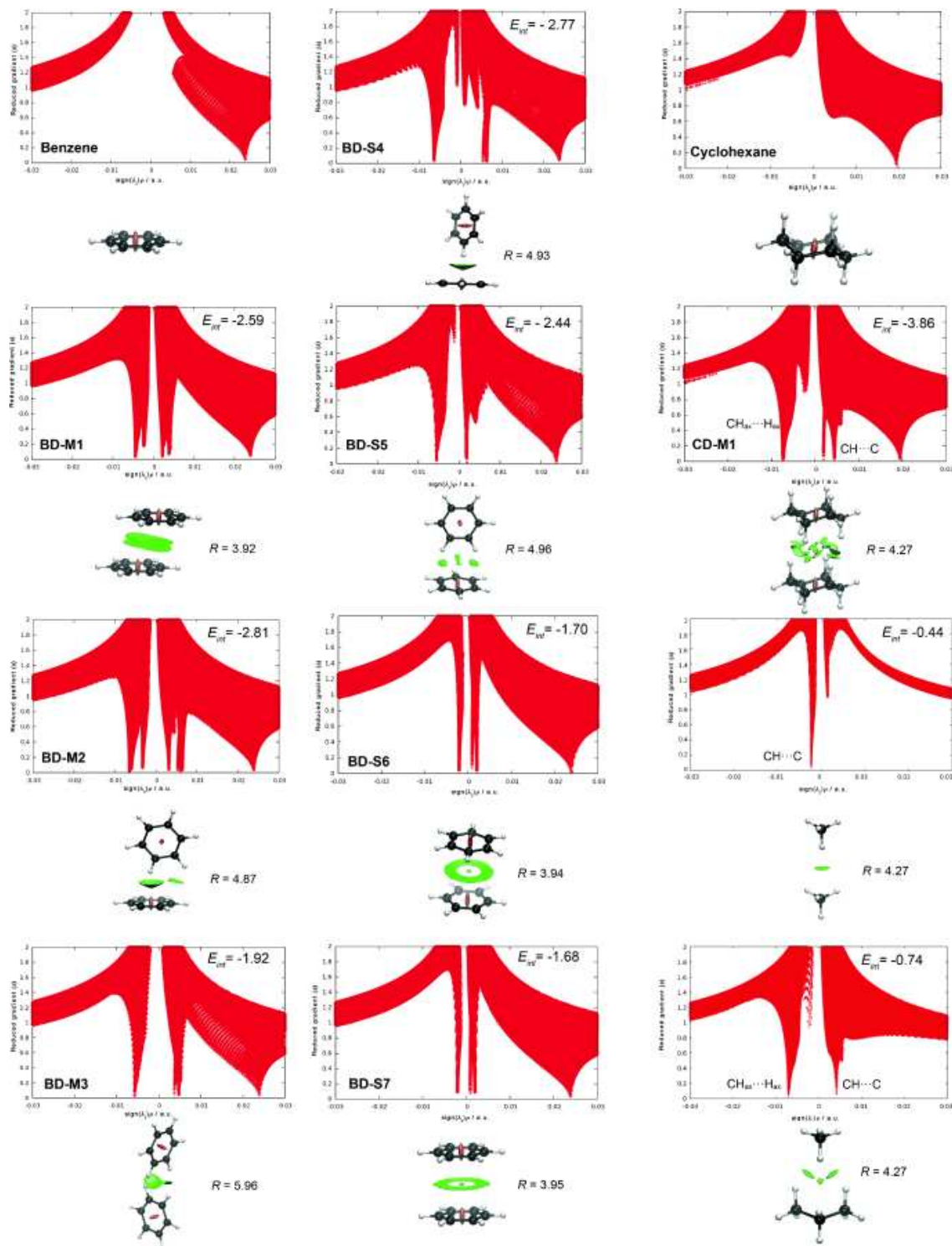
Figure 6.4 displays the computed  $s(\rho)$  diagrams and NCI isosurfaces of the different configurations of the benzene dimer. The interaction peaks appear at density values lower than 0.01 a.u., which corresponds to the region of weak dispersion interactions, characterized by the green color at the isosurfaces. The number and location of repulsive and attractive peaks, together with their area, is highly dependent on the benzene-



6.3 Minima (M) and saddle-points structures (S) of the benzene dimer (BD) and cyclohexane dimer (CD).

dimer configurations. In the parallel-displaced structure BD-M1, a continuous isosurface appears between the overlapping regions of the monomers, corresponding to the  $\pi - \pi$  stacking interaction. The global minimum BD-M2 is characterized by two attractive isosurfaces, corresponding to a CH– $\pi$  interaction and a weaker CH $\cdots$ C dispersion interaction. It is interesting to note that this CH $\cdots$ C dispersion interaction is not found in BD-S4 and the binding energy is therefore slightly smaller, explaining the stability of the distortion of the T-shape.

NCI for the cyclohexane dimer (CD-M1) significantly differs from that of the aromatic benzene dimer. The  $\sigma - \sigma$  stacking interaction is significantly more localized and directional than the  $\pi$ -stacking interaction. Six attractive isosurfaces are located between the axial hydrogen atoms of the different fragments. The short distance between the closest hydrogen atoms of 2.21 Å is responsible for the strong dispersion interactions found in the cyclohexane dimer. It is noteworthy that the closest carbon atoms in BD-M1 are separated by 3.92 Å. A secondary interaction is found between the axial CH bonds of one fragment and the CH<sub>2</sub> moiety of the other monomer [ $d(H_{ax1} \cdots C_2) = 3.12$  Å], although it is significantly weaker. These interactions are exactly the same that would be found in a “truncated” methane $\cdots$ methane dimer and the methane $\cdots$ propane dimer with the equilibrium distances of the cyclohexane dimer.



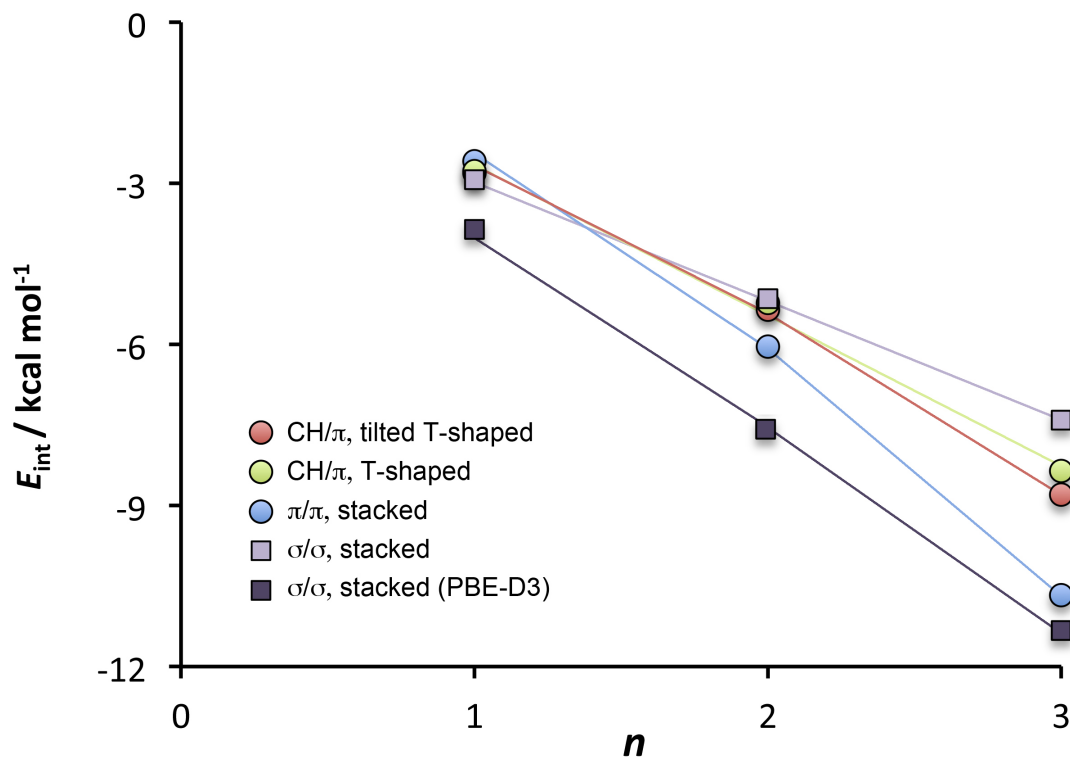
**6.4** NCI analysis of the different configurations of the benzene dimer, the cyclohexane dimer and several  $\sigma - \sigma$  dimers. The gradient isosurfaces ( $s=0.5$  a.u.) are colored on a BGR scale according to the  $\text{sign}(\lambda_2)\rho$  over the range  $-0.03$  to  $0.03$  a.u. Interaction energies ( $E_{int}$  in  $\text{kcal mol}^{-1}$ ) and intermonomer distances ( $R$  in Å) are also shown.



## 6.3.2

## System size

Next step was to investigate the effect of the system size on the strength of the  $\pi - \pi$  and  $\sigma - \sigma$  interactions. Accordingly, we have computed the interaction energies of the naphthalene and anthracene dimers (ND and AD, respectively) and compared them to their respective saturated systems, the decaline and perhydroanthracene dimers (DD and PD). Three different configurations (stacked, tilted T-shaped and T-shaped) were considered for the aromatic dimers, whereas only the trans isomer was computed for the perhydrogenated systems.

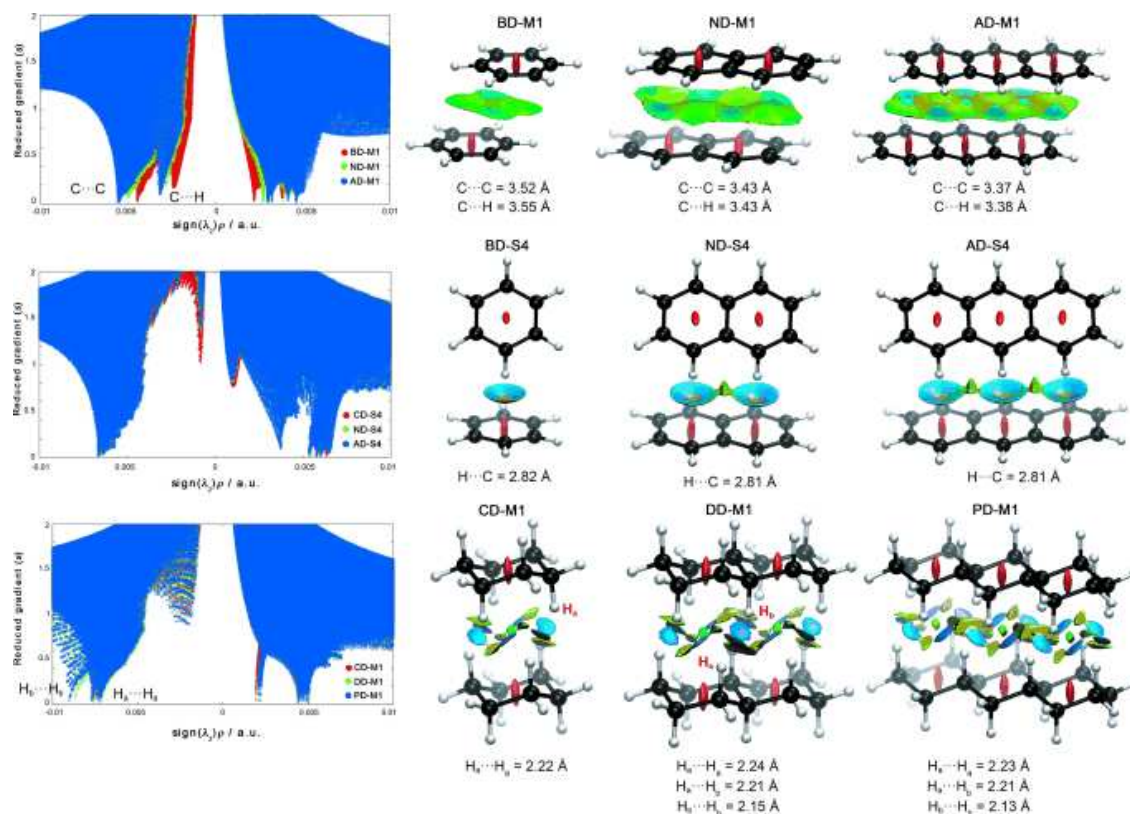


6.5 B97D/aug-cc-pVTZ BSSE-corrected interaction energies ( $E_{int}$  in  $\text{kcal mol}^{-1}$ ) as function of the number of rings ( $n$ ). For the saturated series, the PBE-D<sub>3</sub>/TZ2P interaction energies are also plotted.

According to the interaction energies (Figure 6.5), the  $\sigma - \sigma$  stacking interactions are ca.  $1 \text{ kcal mol}^{-1}$  weaker than the  $\pi - \pi$  stacking for  $n = 2$ . However, for  $n = 3$ , the stacked aromatic dimer are stabilized by ca.  $3 \text{ kcal mol}^{-1}$  relative to the saturated dimer. So the  $\pi - \pi$  stacking interactions stabilize the system more than the  $\sigma - \sigma$  interactions as the number of rings increases. Our results suggest that systems like graphene bilayer, which is a really interesting material for nanotechnology, would be stabilized over saturated systems like the graphane bilayer. Accordingly, at the CC level, graphane dimerization energies were recently shown to be lower than the corresponding  $\pi$ -stacking energies. [137] On the other hand, similar interaction energies are found for the T-shaped structures and the stacked saturated dimers. Therefore, the strength of the  $\pi - \pi$  and  $\sigma - \sigma$  dispersion interactions is similar for small dimers ( $n = 1-2$ ) and only for larger dimers ( $n = 3$ ) stronger interactions are found in the stacked arenes. This fact suggests that for large linear arenes, namely graphene nanoribbons, the stacked conformation will be strongly preferred than a T-shaped arrangement in a bilayer system.

These results about binding energies can be further explained by the NCI method. The NCI isosurfaces computed for the different binding motifs of the naphthalene and anthracene dimers and the corresponding saturated dimers are shown in Figure 6.6. The strengthening of the  $\pi - \pi$  stacking interaction when going from the benzene dimer to the anthracene dimer is clearly visualized with the shift of the characteristic NCI peaks toward bigger density values. Indeed, the NCI peak associated with the  $C \cdots C$  dispersion interaction appears at  $-0.0044$  a.u. in BD-M1 and at  $-0.0056$  a.u. in AD-M1. On the contrary, the NCI peaks of the T-shaped arenes are not shifted as the size of the  $\pi$ -system increases. In this case, only the volume of the  $CH - \pi$  isosurfaces increases. For the  $\sigma - \sigma$  interactions this shift does not happen either, and the position of the NCI peaks remains unaltered for the larger saturated dimers. Nevertheless, a new NCI isosurface appears in DD-M1 and PD-M1, corresponding to the interaction between the hydrogen atoms at the bridgehead carbons ( $H_b$ ).

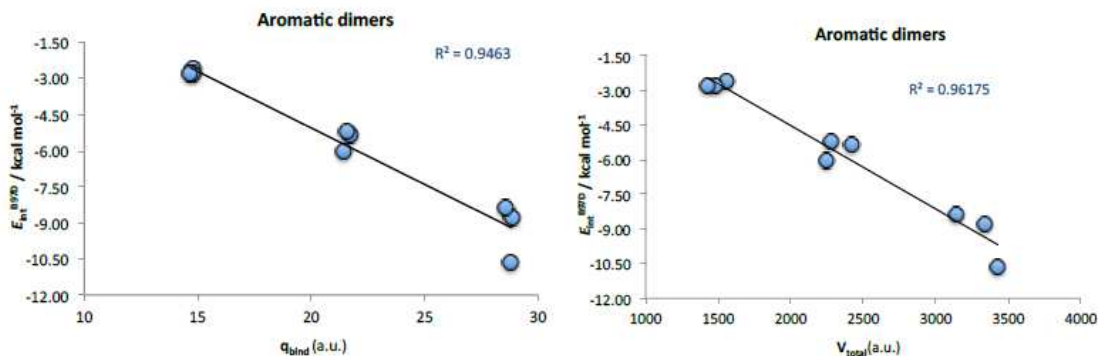
Even more, the largest interaction energies computed for the stacked aromatic dimers are correlated with the increasing density values of the low-gradient spikes and the shortening of the  $C \cdots C$  distances as the number of rings ( $n$ ) increases. However, in the T-shaped dimers and stacked saturated dimers the intermolecular distances and the density values of the peaks remain constant. Accordingly, these two binding motifs show a similar dependence of the interaction energy on system size and both types of interactions are additive. As shown in Figure 6.5, the slope of the  $E_{int}$  with  $n$  is much larger for the stacked aromatic dimers than for the T-shaped and saturated dimers.



**6.6** NCI analysis of the stacked and T-shaped configurations of the benzene, naphthalene and anthracene dimers and the corresponding saturated systems. The gradient isosurfaces ( $s=0.5$  a.u.) are colored on a BGR scale according to the  $\text{sign}(\lambda_2)\rho$  over the range  $-0.01$  to  $0.01$  a.u. Selected intermolecular distances (in Å are also shown).

The NCI analysis reveal that the dispersion between axial hydrogen atoms is responsible for the strong  $\sigma - \sigma$  stacking interactions, whereas the dispersion between carbon atoms is the main attractive contribution

to the  $\pi - \pi$  stacking interactions. In the T-shaped dimers, the  $H \cdots C$  dispersion forces play the major role in the  $\sigma - \pi$  interactions, due to the different spatial arrangement. NCI quantitatively explains the different behavior of the aromatic and saturated stacked dimers as the size of the system increases. Good correlations between the interaction energies and the volumes of the isosurface ( $V_{NCI}$ ) and the integrated charges ( $q_{bind}$ ) are found for the aromatic dimers (Figure 6.7). It can be easily visualized from NCI that  $\sigma - \sigma$  and  $\sigma - \pi$  interactions are local, whereas  $\pi - \pi$  interactions are inherently delocalized, which give rise to a non-additive effect: whereas the interaction energies increases linearly with the size of the system for the  $\sigma - \sigma$  and  $\sigma - \pi$ , the nonlinearity of the curve for the stacked arenes points out to a non-additive effect, which gives rise to a shift of the NCI peaks toward bigger density values and a shortening of the intermolecular distances.



6.7 The correlation between the interaction energies computed with B97D/aug-cc-pVTZ (left) and CCSD(T)/CBS (right) levels of theory and the volume of the NCI region and the integrated binding charge ( $q_{bind}$ ).

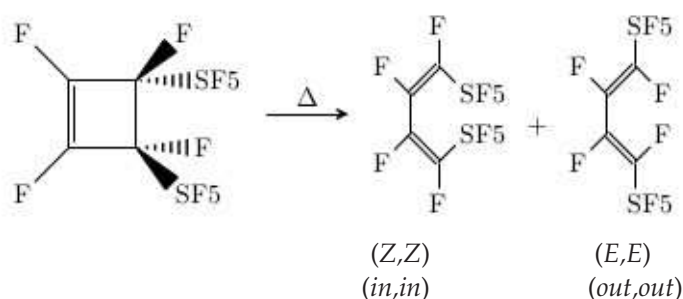
## 7 Some applications

### 7.1

#### Reactivity

Understanding and predicting chemical reactivity are some of the achievements of quantum chemistry. In this regard, the Woodward-Hoffmann rules [21] for pericyclic reactions have become a classical reference. By definition, pericyclic reactions evolve via a cyclic aromatic transition state of delocalized electrons where bond making and bond breaking occur simultaneously in a cyclic array. Using the orbital symmetry conservation, Woodward-Hoffmann proposed a list of rules of thumb able to predict the mechanism and, hence the stereoselectivity of pericyclic reactions. Examples include cycloadditions, electrocyclizations, sigmatropic rearrangements, and chelotropic reactions. Much work has been devoted to show that electron circulation on the pericyclic transition states may be smartly characterized by the topology of the electron localization function (ELF). [138] Recently, it was shown how the combined analysis of the NCI method and ELF may be employed as a visual tool to understand the electron reorganization along an intrinsic reaction path (IRC). [139] Contrary to ELF, the reduced density gradient does not suffer from catastrophes (sudden creation and/or destruction of critical points), being possible to preclude the bonding formation from the first stages of the reaction.

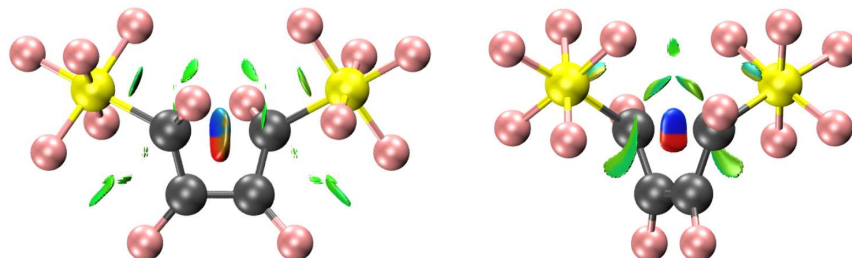
One example of application of NCI to predict the outcome of pericyclic reactions is provided by the thermal ring-opening of *cis*- and *trans*-1,2,3,4-tetrafluoro-1,4-bis(pentafluorosulfanyl)cyclobutene (see Figure 7.1). As a thermal,  $4n$  electron process, the Woodward-Hoffmann rules predict that the conrotatory opening is more favorable than the disrotatory one. [21, 140] Additionally, a given terminal substituent may either rotate "outward", leading to (*E,E*)-1,2,3,4-tetrafluoro-1,4-bis(pentafluorosulfanyl)butadiene or "inward" to yield (*Z,Z*)-1,2,3,4-tetrafluoro-1,4-bis(pentafluorosulfanyl)butadiene. Activation energies obtained at the  $\omega$ B97X-D/6-31G\*\* level for (*E,E*) and (*Z,Z*) transition states are 41.55 kcal/mol and 21.12 kcal/mol, respectively. Because this kind of stereoselectivity is related to the direction of the twist, it was named *torquoselectivity* by Houk and co-workers. [141]



7.1 "Outward" (out) and "inward" (in) conrotatory processes for the thermal ring opening of *trans*-1,2,3,4-tetrafluoro-1,4-bis(pentafluorosulfanyl)cyclobutene.

Rondan and Houk proposed in 1984 a widely accepted orbital model able to explain *torquoselectivity*. [142, 143] In a nutshell, this model states that electron donor substituents at C<sub>3</sub> and C<sub>4</sub> preferentially

rotate outward in order to maximize the stabilizing interaction with the HOMO of the breaking C<sub>3</sub>-C<sub>4</sub> bond and to minimize the repulsive interaction with the LUMO of the same bond. Electron acceptor substituents undergo the opposite effect, and, consequently, inward rotation is preferred. Since only certain orbitals are included in the model, a wrong selection of the interacting orbitals leads to wrong predictions. This disadvantage is common for all theories based on a selected group of orbitals, such as the frontier orbital theory. [144] To avoid this flaw, Ponec decided to reinvestigate the problem in terms of an electron density based indicator, such as the molecular similarity approach. [145] He showed that the origin of the *torquoselectivity* comes from the low electron reorganization required to convert reactants into products.



7.2 NCI isosurfaces of (*E,E*)(left) and (*Z,Z*)(right) transition states.

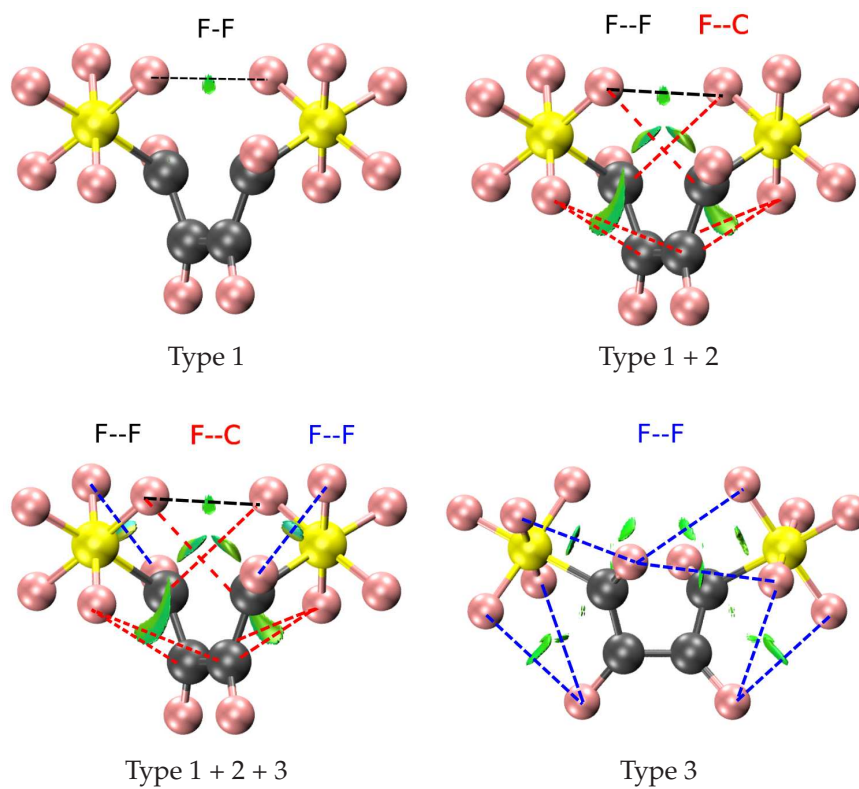
Additionally, NCI analyses of both (*Z,Z*) and (*E,E*) transition states provide us with topological arguments to understand this differential selectivity. As seen in Figure 7.2, out of the breaking carbon-carbon covalent interaction (blue isosurface) and its repulsive counterpart ring tension (red isosurface), we can differentiate three types of noncovalent interactions (green isosurfaces):

**Type 1** Fluor-fluor interaction between pentafluorosulfanyl groups

**Type 2** Pentafluorosulfanyl-carbon interaction

**Type 3** Fluor-fluor interaction between pentafluorosulfanyl and fluoro groups

All of them are present in the (*Z,Z*) transition state, whereas only interactions of type 3 are found in the (*E,E*) one (see Figure 7.3). Thus, dispersion interactions between pentafluorosulfanyl groups and those with the carbon cycle should be the driving force of the process. Thus, *torquoselectivity* can also be understood in terms of secondary interactions as revealed by NCI: within this approach products are driven by the accumulation of noncovalent interactions in the transition state.



**7.3** Noncovalent interactions types in (*Z,Z*) (top left, top right and bottom left) and (*E,E*) (bottom, right) transition states. Black, red and blue dashed lines represent type 1, type 2 and type 3 interactions respectively.

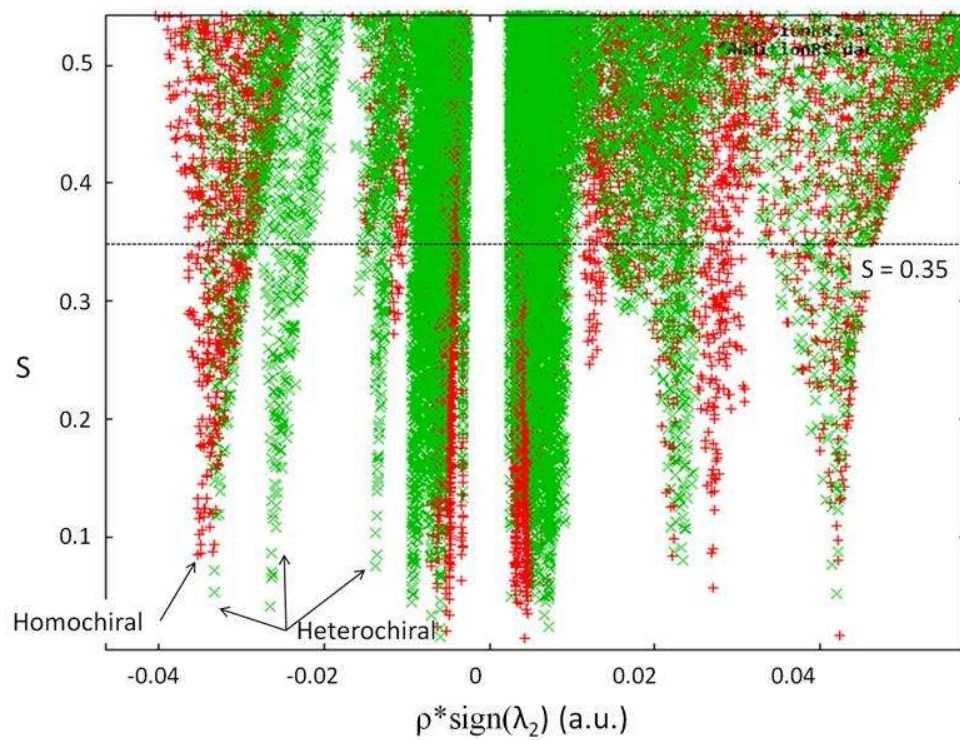
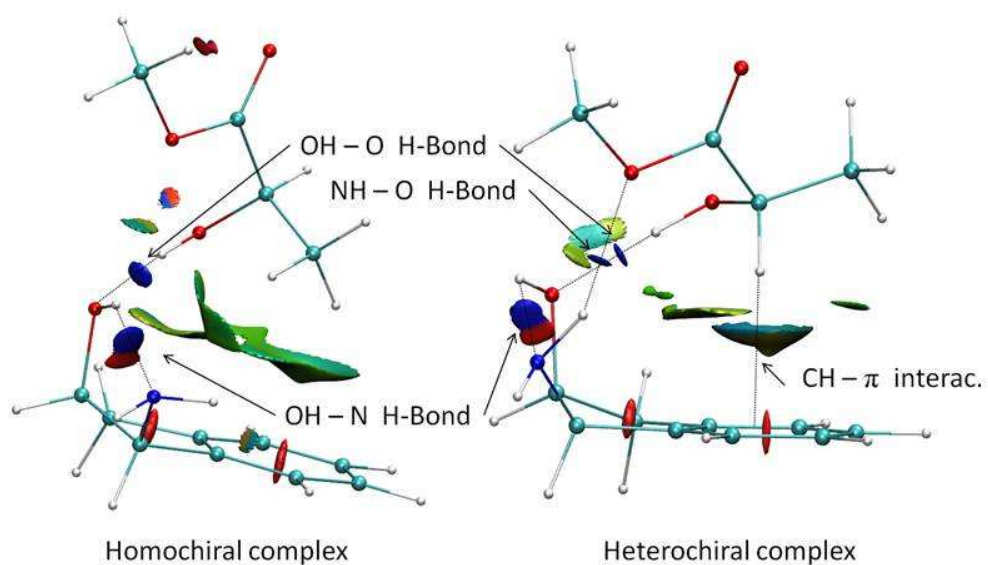
## 7.2

### Chiral recognition

Chiral recognition is thought to happen through the formation of weakly bound complexes involving specific interactions. [146] Chiral recognition results from a subtle balance between plethoras of weak interactions which are difficult to unravel. Especially challenging is the fact that recognition is usually better in less strongly bound complexes, as shown recently in supramolecular chemistry experiments. [148,149] This is related to the fact that chiral recognition is usually not directly related to the strong interaction ensuring the stability of the complex, but results from much weaker specific interactions, such as  $\text{CH} \cdots \pi$ ,  $\text{CH} \cdots \text{O}$ , or differences in dispersion between the two enantiomers. There is therefore a need for theoretical methods, such as NCI, enabling the visualization of weak interactions and their dependence upon chirality.

We present here an example of chiral recognition in a neutral complex, the (1*R*,2*R*)-(-)-cis-1-amino-2-indanol (AI) - methyl lactate (ML) complex, which has been extensively studied by IR-UV double resonance experiments. [147,150,151] It has been observed that the heterochiral complex is more stable than the homochiral.

Visual examination of Figure 7.4 enables to visualize this interaction. Indeed, changing the methyl-lactate's chirality only consists in swapping the H atom on the asymmetric carbon, and the methyl group. This change introduces repulsion, prevents the formation of a  $\text{CH} \cdots \pi$  interaction, and decreases the binding energy by 2 kcal/mol, a value usually associated with  $\text{CH} \cdots \pi$  interactions. However, no direct evidence of this critical interaction was possible so far because it has only limited and hardly predictable consequences on the  $\nu(\text{CH})$  stretch frequency. [152,153]



7.4 2D-NCI plots (top) and 3D-NCI plots (bottom) of the heterochiral (left) and homochiral (right) (1*R*,2*R*)-(-)-*cis*-1-amino-2-indanol - methyl lactate complexes.





## 8 Summary and conclusions

In conclusion, non-covalent interactions have a unique signature and their presence can be revealed solely from the electron density. Noncovalent interactions are highly nonlocal and manifest in real space thanks to the NCI analysis: in other words, as low-gradient isosurfaces with low densities. The sign of the second Hessian eigenvalue is used to identify the interaction type, and its strength can be derived from the density on the non-covalent interaction surface.

NCI provides a rapid and rich representation of van der Waals interactions, hydrogen bonds, and steric clashes. If obliged by the size of the system, NCI can be approximated from promolecular densities, so that it only requires the atomic coordinates as input. Thus, it is applicable to large systems, such as proteins or DNA. Since it is based on the electron density, it is applicable to all types of chemical bonds. We have reviewed here several such examples, which go even beyond the original definition, such as ionic or covalent bonding. We have also shown the ability of NCI to provide a global approach to AIM, which allows to overcome its limitations when the yes-no bcp criterion becomes too strict.

Energy arises as a main issue in this HDR, where individual cases are reviewed, revealing binding energy potentials for hydrogen bonds, and conformational analysis for interactions as subtle as the ones in benzene dimer and its related families.

Finally, we have looked at the change of chemical interactions along a reaction path, reformulating orbital rules in the torquoselectivity. In summary, we have shown that the electron density and its derivatives contain all the information needed to characterize all chemical bonds and their change, making NCI a holistic tool in the analysis of weak (and not so weak) interactions.

## Bibliography

- 1 L. Pauling. 1947. *General Chemistry*, Dover Publications, Inc.
- 2 J. K. Burdett. 1997. *Chemical Bonds-A Dialog*. Wiley: Chichester, England.
- 3 G. Frenking, and S. Shaik (editors). 2007. *Journal of Computational Chemistry* 28:1.
- 4 G. Frenking, and A. Krapp. 2007. *Journal of Computational Chemistry* 28:15.
- 5 S. Shaik, H. S. Rzepa, and R. Hoffmann. 2013. *Angewandte Chemie International Edition* 52:3020.
- 6 G. Frenking, and M. Hermann. 2013. *Angewandte Chemie International Edition* 52:5922.
- 7 C. A. Coulson. 1953. *The Spirit of Applied Mathematics*, Clarendon Press.
- 8 H. Jacobsen. 2010. *Dalton Transactions* 39:5426.
- 9 R. G. Parr, P. W. Ayers, and R. F. Nalewajski. 2005. *The Journal of Physical Chemistry A* 109:3957.
- 10 H. Jacobsen. 2013. *Physical Chemistry Chemical Physics* 15:5057.
- 11 P. v. R. Schleyer. 2005. *Chemical Reviews* 105:3433.
- 12 P. L. A. Popelier. 2007. *Faraday Discussions* 135:1.
- 13 I. V. Alabugin, K. M. Gilmore, and P. W. Peterson. 2011. *Wiley Interdisciplinary Reviews: Computational Molecular Science* 1:109.
- 14 J. F. Gonthier, S. N. Steinmann, M. D. Wodrich, and C. Corminboeuf. 2012. *Chemical Society Reviews* 41:4671.
- 15 A. Whitaker. *Einstein, Bohr and the Quantum Dilemma*. 1996. Cambridge. Cambridge University Press.
- 16 S. Alvarez, R. Hoffmann, and C. Mealli. 2009. *Chemistry-A European Journal* 15:8358.
- 17 D. Danovich, P. C. Hiberty, W. Wu, H. S. Rzepa, and S. Shaik. 2014. *Chemistry-A European Journal* 20:6214.
- 18 P. L. Ayers, R. J. Boyd *et al.* 2015. *Computational and Theoretical Chemistry* 1053: 2.
- 19 G. N. Lewis. 1916. *J. Am. Chem. Soc.* 38:762-786.
- 20 K. Fukui, T. Yonezawa, and H. Shingu. 1952. *Journal of Chemical Physics* 20:722.
- 21 R. B. Woodward, and R. Hoffmann. 1969. *Angew. Chem., Int. Ed. Engl.* 8:781.
- 22 R. G. Parr, R. A. Donnelly, M. Levy, and W. E. Palke. 1978. *Journal of Chemical Physics* 68:3801.
- 23 R. F. W. Bader. 1991. *Chem. Rev.* 91:893.
- 24 R. F. W. Bader. *Atoms in Molecules: A Quantum Theory*. 1990. Oxford. International Series of Monographs on Chemistry 22; Oxford Science Publications.
- 25 C. F. Matta, and R. J. Boyd. *In The Quantum Theory of Atoms in Molecules*. 2007. New York. Wiley-VCH.
- 26 A. D. Becke, and K. E. J. Edgecombe. 1990. *J. Chem. Phys.* 92: 5397.
- 27 B. Silvi, and A. Savin. 1994. *Nature* 371:683.
- 28 B. Honig, and A. Nicholls. 1995. *Science* 268:1144.
- 29 P. A. Kollman. 1977. *Chem. Rev.* 10:365.
- 30 H. Fenniri, M. Packiarajan, K. L. Vidale, D. M. Sherman, K. Hallenga, K. V. Wood, J. G. Stowell. 2001. *J. Am. Chem. Soc.* 123:3854.
- 31 P. Kruse, E. R. Johnson, G. A. DiLabio, R. A. Wolkow. 2002. *Nano Lett.* 2:807.
- 32 S. S. Sheiko, F. C. Sun, A. Randall, D. Shirvanyants, M. Rubinstein, H. Lee, K. Matyjaszewski. 2006. *Nature*. 440:191.
- 33 G. A. DiLabio, P. G. Piva, P. Kruse, R. A. Wolkow. 2004. *J. Am. Chem. Soc.* 126:16048.
- 34 J. Cerniý, P. Hobza. 2007. *Phys. Chem. Chem. Phys.* 9:5291.
- 35 A. L. Lehninger, D. L. Nelson, M. M. Cox. 1993. *Principles of Biochemistry. Second edition*. Worth Publishers, Inc.
- 36 N. Krishnamoorthy, M. H. Yacoub, S. N. Yaliraki. 2011. *Bio-materials* 32:7275.
- 37 A. Dutta, A. D. Jana, S. Gangopadhyay, K. Kumar Das, J. Marek, R. Marek, J. Brus, M. Ali. 2011. *Phys. Chem. Chem. Phys.* 13:15845.
- 38 A. Gavezzotti. *Molecular Aggregation. Structure Analysis and Molecular Simulation of Crystals and Liquids*. 2007. Oxford. IUCr monographs on Crystallography n. 19, Oxford University Press.
- 39 S. Keinan, M. A. Ratner, T. J. Marks. 2004. *J. Chem. Phys. Lett.* 392:291.
- 40 G. R. Desiraju. *Crystal Engineering. The design of organic Solids* 1989. Amsterdam. Elsevier.
- 41 G. M. Day *et al.* 2009. *Acta Cryst. B.* 65:107.
- 42 J. M. Word, S. C. Lovell, T. H. LaBean, H. C. Taylor, M. E. Zalis, B. K. Presley, J. S. Richardson, and D. C. Richardson. 1999. *J. Mol. Biol.* 285:1735.
- 43 I. W. Davis, A. Leaver-Fay, V. B. Chen, J. N. Block, G. J. Kapral, X. Wang, L. W. Murray, W. B. Arendall III, J. Snoeyink, J. S. Richardson, and D. C. Richardson. 2007. *Nucleic Acids Res.* 35:W375.
- 44 V. Sobolev, A. Sorokine, J. Prilusky, E. E. Abola, and M. Edelman. 1999. *Bioinformatics* 15:327.
- 45 I. K. McDonald, and J. M. Thornton. 1994. *J. Mol. Biol.* 238:777.
- 46 M.E. Alikhani, F. Fuster, and B. Silvi. 2005. *Struct. Chem.* 16:203.
- 47 R. D. Cramer III, D. E. Patterson, and J. D. Bunce. 1988. *J. Am. Chem. Soc.* 110:5959.
- 48 J. Pilmé, J.-P. Piquemal. 2008. *J. Comput. Chem.* 29:1440.
- 49 P. Hohenberg, and W. Kohn. 1964. *Phys. Rev. B* 136:B864.
- 50 E. R. Johnson, S. Keinan, P. Mori-Sanchez, J. Contreras-García, A. J. Cohen, and W. Yang. 2010. *J. Am. Chem. Soc.* 132:6498.
- 51 J. Contreras-García, E. Johnson, S. Keinan, R. Chaudret, J.-P. Piquemal, D. Beratan, and W. Yang. 2011. *J. Chem. Theor. Comp.* 7:625.
- 52 J. Contreras-García, E. R. Johnson, W. Yang. 2011. *J. Phys. Chem. A* 115:12983.
- 53 A. D. Becke. 1995. World Scientific, Yarkony.
- 54 A. J. Cohen, P. Mori-Sánchez, and W. Yang. 2008. *Science* 321:792.
- 55 A. Zupan, K. Burke, M. Ernzerhof, J. P. Perdew. 1997. *J. Chem. Phys.* 106:10184.
- 56 A.D. Becke. 1993. *J. Chem. Phys.* 98:5648.
- 57 C. Lee, W. Yang, and R.G. Parr. 1988. *Phys. Rev. B.* 37:785.
- 58 G. Arfken, G. *Mathematical Methods for Physicists*. 1985. Orlando Academic Press.
- 59 R. F. W. Bader, H. Essén. 1984. *J. Chem. Phys.* 80:1943.

- 60 J. R. Lane, J. Contreras-García, J.-P. Piquemal, B. J. Miller, and H. G. Kjaergaard. 2013. *J. Chem. Theory Comp.* 9:3263.
- 61 J. Contreras-García, M. Calatayud, J.-P. Piquemal, and J. M. Recio. 2012. *Comp. Theo. Chem.* 998:193.
- 62 R. Chaudret, B. de Courcy, J. Contreras-García, E. Gloaguen, A. Zehnacker-Rentien, M. Mons, and J.-P. Piquemal. 2013. *Phys. Chem. Chem. Phys.* 16:9876.
- 63 M. A. Spackman, E. N. Maslen. 1986. *J. Phys. Chem.* 90:2020.
- 64 A. Martín Pendás, V. Luaña, L. Pueyo, E. Francisco, P. Morisánchez. 2002. *J. Chem. Phys.* 117:1017.
- 65 S. Fiedler, J. Broecker, S. Keller. 2010. *Cellular and Molecular Life Sciences*, 67:1779.
- 66 K. A. Dill. 1990. *Biochemistry*, 29:7133.
- 67 B. J. Deppmeier, A. J. Driessen, W. Hehre, J. A. Johnson, P. E. Klunzinger, and M. Watanabe. 2002. *Spartan ES 1.0.2*. Wavefunction Inc., Irvine.
- 68 X.-J. Lu, and W. K. Olson. *Nucleic Acids Res.* 31:5108.
- 69 <http://rutchem.rutgers.edu/~olson/Tsukuba/>.
- 70 E. Espinosa, E. Molins, C. Lecomte. 1988. *Chem. Phys. Lett.* 285:170.
- 71 R. Wiczorek, J. J. Dannenberg. 2004. *J. Am. Chem. Soc.* 126:14198.
- 72 R. Viswanathan, A. Asensio, and J. J. Dannenberg. 2004. *J. Phys. Chem. A*. 108:9205.
- 73 P. Jurecka, and P. Hobza. 2003. *J. Am. Chem. Soc.* 125:15608.
- 74 A. M. Pendás, A. Costales, V. Luaña. 1998. *J. Phys. Chem. B*, 102:6937.
- 75 J. Cioslowski, S. T. Mixon. 1992. *Can. J. Chem.*, 70:443.
- 76 C. F. Matta, J. Hernandez-Trujillo, T. Tang, R. F. W. Bader. 2003. *Chem. Eur. J.*, 9:1940.
- 77 M. E. Alikhani, F. Fuster, B. Silvi. 2005. *Struct. Chem.*, 6:203.
- 78 D. L. Howard, P. Jorgensen, H. G. Kjaergaard. 2005. *J. Am. Chem. Soc.*, 127:17096.
- 79 D. L. Howard, H. G. Kjaergaard. 2006. *J. Phys. Chem. A*, 110:10245.
- 80 H.-J. Werner, P. Knowles, G. Knizia, F. R. M. S. F. R. Manby, P. Celani, T. Korona, R. Lindh, A. Mitrushenkov, G. Rauhut, K. Samasundar, T. Adler, R. D. Amos, A. Bernhardsson, A. Berning, D. L. Cooper, M. J. O. Deegan, A. J. Dobbyn, F. Eckert, E. Goll, C. Hampel, A. Hesselmann, G. Hetzer, T. Hrenar, G. Jansen, C. Koppl, Y. L. A. W. Llyoyd, R. A. Mata, A. J. May, S. J. McNicholas, W. Meyer, M. E. Mura, A. Nicklass, D. P. O'Neill, P. Palmieri, D. Peng, K. Pfluger, R. Pitzer, M. Reiher, T. Shiozaki, H. Stoll, A. J. Stone, R. Tarroni, T. Thorsteinsson, M. Wang. 2010. *MOLPRO*. University College Cardiff Consultants Limited: Cardiff, U. K.
- 81 K. A. Peterson, T. B. Adler, H.-J. Werner. 2008. *J. Chem. Phys.*, 128:084102.
- 82 J. R. Lane, H. G. Kjaergaard. 2009. *J. Chem. Phys.*, 131:034307.
- 83 F. R. Manby. 2003. *J. Chem. Phys.*, 119:4607.
- 84 H.-J. Werner, T. B. Adler, F. R. Manby. 2007. *J. Chem. Phys.*, 126:164102.
- 85 F. Weigend, A. Kohn, C. Hattig. 2002. *J. Chem. Phys.*, 116:3175.
- 86 F. Weigend. 2002. *Phys. Chem. Chem. Phys.*, 4:4285.
- 87 K. E. Yousef, K. A. Peterson. 2008. *J. Chem. Phys.*, 129:184108.
- 88 W. Zhou. 2012. *MOLDEN2AIM*. <http://people.smu.edu/wzou/>.
- 89 A. K. Todd. 2012. *AIMAll*. TK Gristmill Software. <http://aim.tkgristmill.com/index.html>.
- 90 B. R. Henry, H. G. Kjaergaard. 2002. *Can. J. Chem.*, 80:1635.
- 91 D. L. Howard, P. Jorgensen, H. G. Kjaergaard. 2005. *J. Am. Chem. Soc.*, 127:17096.
- 92 B. J. Miller, J. R. Lane, H. G. Kjaergaard. 2011. *Phys. Chem. Chem. Phys.*, 13:14183.
- 93 J. F. Dobson, K. McLennan, A. Rubio, J. Wang, T. Gould, H. M. Lee, B. P. Dinte. 2001. *Aust. J. Chem.*, 54:513.
- 94 D. F. T. A. P. I. D. S. Sholl, J. A. Steckel. 2009. *Density Functional Theory: A Practical Introduction*. Wiley, New York.
- 95 L. L. Di Presti, A. Ellern, R. Destro, B. Lunelli. 2009. *J. Phys. Chem. A*, 113:3186.
- 96 R. F. W. Bader. 2009. *J. Phys. Chem. A*, 113:10391.
- 97 R. F. W. Bader. 2010. *J. Phys. Chem. A*, 114:7431.
- 98 A. O. de-la Roza, M. Blanco, A. Pendás, V. Luana. 2009. *Comput. Phys. Commun.*, 180:157.
- 99 A. O. de-la Roza, M. Blanco, A. Pendás, V. Luana. 2009. *Comput. Phys. Commun.*, 180:157.
- 100 P. Giannozzi, S. Baroni, N. Bonini, M. Calandra, R. Car, C. Cavazzoni, D. Ceresoli, G. Chiarotti, M. Cococcioni, I. Dabo, et al. 2009. *J. Phys.: Condens. Matter*, 21:395502.
- 101 X. Gonze, J. Beuken, R. Caracas, F. Detraux, M. Fuchs, G. Rignanesse, L. Sindic, M. Verstraete, G. Zerah, F. Jollet, et al. 2002. *Comput. Mater. Sci.*, 25:478.
- 102 X. Gonze. 2005. *Z. Kristallogr.*, 220:558.
- 103 G. Kresse, J. Furthmüller. 1996. *Comput. Mat. Sci.*, 6:15.
- 104 G. Kresse, J. Furthmüller. 1996. *Phys. Rev. B*, 54:11169.
- 105 K. Schwarz, P. Blaha, G. K. H. Madsen. 2002. *Comput. Phys. Commun.*, 147:71.
- 106 K. Schwarz, P. Blaha. 2003. *Comput. Mater. Sci.*, 28:259.
- 107 K. Dewhurst, S. Sharma, et al. <http://elk.sourceforge.net/>.
- 108 A. M. P. V. Luaña, J. Recio, E. Francisco, M. Bermejo. 1993. *Comput. Phys. Commun.*, 77:107.
- 109 M. J. Frisch, G. W. Trucks, H. B. Schlegel et al. 2009. *Gaussian 09 Rev. A.1*. Gaussian Inc., Wallingford CT.
- 110 A. Kokalj. 1999. *Journal of Molecular Graphics and Modelling*, 17:176.
- 111 G. Henkelman, A. Arnaldsson, H. Jónsson. 2006. *Comput. Mater. Sci.*, 36:354.
- 112 E. Sanville, S. Kenny, R. Smith, G. Henkelman. 2007. *J. Comp. Chem.*, 28:899.
- 113 W. Tang, E. Sanville, G. Henkelman. 2009. *J. Phys.: Condens. Matter*, 21:084204.
- 114 H. R. Allcock, R. L. Kugel, E. G. Stroh. 1972. *Inorg. Chem.*, 11:1120.
- 115 V. Luana, A. Pendás, A. Costales, G. Carriedo, F. García-Alonso. 2001. *J. Phys. Chem. A*, 105:5280.
- 116 A. Gavezzotti. 2008. *Mol. Phys.*, 106:1473.
- 117 L. Denner, P. Luger, J. Buschmann. 1988. *Acta Cryst. C*, 44:1979.
- 118 E. Aubert, S. Lebegue, M. Marsman, T. T. T. Bui, C. Jelsch, S. Dahaoui, E. Espinosa, J. G. Angyán. 2011. *J. Phys. Chem. A*, 115:14484.
- 119 X.-r. c. d. P. Coppens, chemical bonding. 1997. *X-ray charge densities and chemical bonding*. Oxford University Press, USA.

- 120 P. Coppens. 2005. *Angew. Chem. Intl. Ed.*, 44:6810.
- 121 T. Koritsanszky , P. Coppens. 2001. *Chem. Rev.*, 101:1583.
- 122 C. Gatti, R. Bianchi, R. Destro, , F. Merati. 1992. *J. Mol. Struct.: THEOCHEM*, 255:409.
- 123 A. Volkov, Y. Abramov, P. Coppens, , C. Gatti. 2000. *Acta Crystallogr. Sect. A*, 56:332.
- 124 N. K. Hansen , P. Coppens. 1978. *Acta Crystallogr. Sect. A*, 34:909.
- 125 A. Volkov, P. Macchi, L. Farrugia, C. Gatti, P. Mallinson, T. Richter, T. Koritsanszky. 2006. *XD2006-A Computer Program Package for Multipole Refinement, Topological Analysis of Charge Densities and Evaluation of Intermolecular Energies from Experimental and Theoretical Structure Factors*.
- 126 M. L. Waters. 2013. *Acc. Chem. Res.*, 46:873.
- 127 L. M. Salonen, M. Elleremann, , F. Diederich. 2011. *Angew. Chem. Intl. Ed.*, 50:4808.
- 128 S. E. Wheeler. 2013. *Acc. Chem. Res.*, 46:1029.
- 129 R. K. Raju, J. W. G. Bloom, Y. An, , S. E. Wheeler. 2011. *Chem. Phys. Chem.*, 12:3116.
- 130 S. Li, Y. Xu, Q. Shen, X. Liu, J. Lu, Y. Chen, T. Lu, C. Luo, X. Luo, M. Zheng, , H. Jiang. 2013. *Curr. Pharm. Des.*, 19:6522.
- 131 S. Grimme. 2008. *Angew. Chem. Intl. Ed.*, 47:3430.
- 132 J. W. G. Bloom , S. E. Wheeler. 2011. *Angew. Chem. Intl. Ed.*, 50:7847.
- 133 A. A. Fokin, D. Gerbig, , P. R. Schreiner. 2011. *J. Am. Chem. Soc.*, 133:20036.
- 134 C. D. Sherrill. 2013. *Acc. Chem. Res.*, 46:1020.
- 135 O. Bludský, M. Rubeš, P. Soldán, , P. Nachtigall. 2008. *J. Chem. Phys.*, 128:114102.
- 136 R. Podeszwa, R. Bukowski, , K. Szalewicz. 2006. *J. Phys. Chem. A*, 110:10345.
- 137 T. Janowski , P. Pulay. 2012. *J. Am. Chem. Soc.*, 134:17520.
- 138 E. Matito, J. Poater, M. Duran, and M. Sola. 2006. *Eur. J. Chem. Phys. Phys. Chem.*, 7:111.
- 139 N. Gillet, R. Chaudret, J. Contreras-Garcia, W. Yang, B. Silvi, and J.-P. Piquemal. 2012. *J. Chem. Theo. Comp.*, 8:3993.
- 140 R. B. Woodward, R. J. Hoffmann. 1965. *J. Am. Chem. Soc.*, 87:2046.
- 141 K. N. Houk, Y. Li, and J. D. Evanseck. 1992. *Ang. Chem. Intl Ed.*, 31:682.
- 142 W. Kirmse, N. G. Rondan, and K. N. Houk. 1984. *J. Am. Chem. Soc.*, 106:7989.
- 143 N. G. Rondan, K. N. Houk. 1984. *J. Am. Chem. Soc.*, 107:2099.
- 144 M. J. S. Deward. 1989. *J. Mol. Struct.* 200:301.
- 145 R. Ponec, G. Yuzhakov, and J. Pecka. 1996. *J. Math. Chem.*, 20:301.
- 146 W. H. Pirkle , T. C. Pochapsky. 1989. *Chem. Rev.*, 89:347.
- 147 R. F. W. Bader. 1991. *Chem. Rev.*, 91:893.
- 148 A. Bouchet, T. Brotin, M. Linares, H. Agren, D. Cavagnat, , T. Buffeteau. 2011. *J. Org. Chem.*, 76:4178.
- 149 E. Gloaguen, H. Valdes, F. Pagliarulo, R. Pollet, B. Tardivel, P. Hobza, F. o. Piuzzi, , M. Mons. 2009. *J. Phys. Chem. A*, 114:2973.
- 150 Z. Arp, N. Meinander, J. Choo, , J. Laane. 2002. *J. Chem. Phys.*, 116:6648.
- 151 K. L. Barbu-Debus, F. Lahmani, A. Zehnacker-Rentien, , N. Guchhait. 2006. *Chem. Phys. Lett.*, 422:218.
- 152 S. Tsuzuki , A. Fujii. 2008. *Phys. Chem. Chem. Phys.*, 10:2584.
- 153 S. Tsuzuki, K. Honda, A. Fujii, T. Uchimaru, , M. Mikami. 2008. *Phys. Chem. Chem. Phys.*, 10:2860.

**Part II**  
**Research Project**

# Research Project

The analysis of non covalent interactions with the help of NCI is a very young, though already productive field, which the applicant will continue to develop the theory behind it in the coming years.

With this, she will aim at

- 1) creating both a universal language (bond definition) and quantitative framework (energetics) for describing non-covalent interactions,
- 2) implementing a new code, which includes all new developments and which is easier to use at all levels, and
- 3) use these results, which arise in critically important and diverse chemical contexts for solids and biosystems.

## Aims

### 1. Extending the model

NCI being a young tool, one of the first step that is needed for a coherent and well set use of the reduced density gradient as identifier of non covalent interactions is the definition of a universal language within this framework. At all points, comparison with previously existing (QTAIM, ELF) topological analysis of the chemical bond will be carried out, in search for (in)coherencies.

- **Language:** A new topological definition of weak interactions will be reviewed from the NCI point of view.

-Unconventional hydrogen bonds. We will analyze unconventional hydrogen bonds, with C-H bonds as unconventional donors,  $\pi$  electrons or simple C-atoms as unconventional acceptors or even the mixture of both, such as C-H $\cdots$ C (or C-H $\cdots\pi$ ) systems or the dihydrogen bonds (X-H $^+ \cdots$ -H-M systems where M-H is a metalhydride bond behaving as an acceptor). Also strong HBs will be investigated. It is known that very strong O-H $\cdots$ O bonds can occur because of severe intramolecular strain; in connection with protonated oxyanions  $^-$ O-H $\cdots$ O $^-$  and due to the fact that the neutral donor and acceptor atoms are connected by a system of  $\pi$ -conjugated double bonds.

-Steric crowding. A topological definition of steric crowding will be envisaged. NCI constitutes one of the first topological descriptors to provide a picture of steric crowding as it has already been known and characterized for a long time. During the next years I will study the steric hindrance in the following cycle series: cyclopropane, cyclobutane, cyclopentane, cyclohexane and analyze their NCI characteristics (absent in AIM) in relationship with experimental and theoretical results.

-Agostic interactions. Agostic interactions characterize interactions of a coordinatively-unsaturated transition metal with a C-H bond, when the two electrons involved in the C-H bond enter the empty  $d$ -orbital of a transition metal, resulting in a three-center two-electron bond. The agostic bond has been characterized extensively in Titanium complexes, in terms of electron density using QTAIM and ELF, and these and similar examples will be used as model system for describing these interactions.

-Cation- $\pi$  and Anion- $\pi$  interactions. Cation- $\pi$  interactions are involved in Na $^+$  and K $^+$  voltage-gated channel. The inverse interaction, the contact between an anion and the face of an electron-poor aromatic ring is also being applied in the design of highly selective anion receptors and channels. The binding of singly-charged small cationic species (p.e. alkali cations) with different aromatic rings, including the aromatic amino acids, will be analyzed. Several complexes will be used as a prototype of the anion- $\pi$  interaction, including different anions (F $^-$ , Br $^-$ , Cl $^-$ , NO $_3^-$ , N $_3^-$ ) and arenes (benzene, hexafluorobenzene, pyridine, pyrazine and triazine).

-Lone pair- $\pi$  interactions. The  $\pi$  electron cloud of aromatic centers can counterintuitively interact in a stabilizing manner with lone pairs. Indeed, this type of interactions has gained attention recently and their role in biomolecular structures is being recognized. We will study various structures of benzene $\cdots$ water, benzene $\cdots$ dimethylether, and 1,2,4,5-tetracyanobenzene $\cdots$ water complexes.

-Halogen bonding. Halogen bonding characterizes the interaction between a halogen atom, acting as a Lewis acid, and a Lewis base. Essentially, the halogen atoms acts like the hydrogen bond in the hydrogen bonds and mutual penetration is observed. However an important difference appears, since halogen atoms are Lewis bases, a halogen atom can both donate and accept a halogen bond. Halogens most typically participating in halogen bonding are Cl, Br and I; sometimes F. They are known to follow the general trend:  $F < Cl < Br < I$ , with iodine normally forming the strongest interactions. These series will be used as test cases.

- **Energetics:** Due to the small changes in electron density upon weak bond formation, these systems constitute a perfect test-bed for the analysis of changes in structure/density and energetics. Given the fact that NCI is able to characterize both favorable and unfavorable interactions in real space, it encloses all the needed ingredients for identifying the changes in electron density which give rise to molecular stabilization. Moreover, the ability of NCI to associate regions in real space to non covalent interactions enables the analysis of global properties of these regions, which are subject to change in a quantifiable manner. During the last years, the applicant has uniquely defined interaction volumes, within which density-based integrations can be performed to obtain properties associated solely with the interacting region (Section 6.2). She has shown that the evolution of these quantities along the potential-energy surface reproduce the interplay of attractive and repulsive interactions seen throughout hydrogen-bond formation. Integration of charges within the interacting region has been shown to mimic very closely the interatomic potentials of conventional hydrogen bonds. This information extracted from 3D will be extremely relevant when analyzing the structural stability of large systems, and of course crucial for understanding their reactivity. We will use two approaches:

-Simple model systems. Simple model systems, with few MO's will be used to understand the relationship between NCI-MO's-Energy. We will start with a decomposition of NCI in terms of MO and use a minimal basis set for processes such as bond formation or excitation to understand the basic effects on the density.

-Rotational barriers. An interesting debate regarding the ultimate nature of the rotation barriers in ethane and other simple systems followed a Nature paper [*Nature*, 431, 565 (2001)] which claimed that hyperconjugation, not steric repulsion, was its final cause. This work, which used a NBO energetic analysis, was immediately contested from several theoretical fronts. We will analyze the relationship between NCI regions in ethane, peroxides and azides in order to set the basis for understanding the interplay between attractive and repulsive interactions which give rise to their rotation barriers.

-General fitting from training sets. Once insight has been gained into the equilibrium between attractive and repulsive forces that determine conformational stability (stretching, rotation), different molecules will come into play to check the capability of NCI to cast the energy of different interacting groups. From the QTAIM point of view, a wealth of investigations has been devoted to analyze the relationship between the geometry of weakly bound dimers and their binding energy. Different measures of H-bond strength based on X-H proton donating bond properties and on parameters of H...Y distance (Y-proton acceptor within X-H...Y H bridges) and density properties have been investigated in order to find correlations between such measures and H-bond energy. Given the fact that NCI collects information from one whole region instead of just local information, it is expected that a smaller number of parameters is needed in order to correlate the binding energy of complexes with NCI properties.

-Reactivity: Understanding and predicting chemical reactivity are some of the achievements of quantum chemistry. In this regard, the Woodward-Hoffmann (WH) rules for pericyclic reactions have become a classical reference. By definition, pericyclic reactions evolve via a cyclic aromatic transition state of delocalized electrons where bond making and bond breaking occur simultaneously in a cyclic array. Using the orbital symmetry conservation, WH proposed a list of rules of thumb able to predict the mechanism and, hence the stereoselectivity of pericyclic reactions. Examples include cycloadditions, electrocyclizations, sigmatropic rearrangements, and cheletropic reactions. However, general



rules that apply to concerted and pseudopericyclic reactions have not yet been found on MO grounds. We expect secondary interactions to play a major role here, and so NCI should be able to shed some light on these examples and generalize the WH rules to pseudo-pericyclic reactions.

## 2. Implementation

Visualization is a main way of diffusion of results due to its intuitive nature. This is one of the greatest advantages of NCI, that is provides a visual approach to something which up to now was elusive. In order to continue with this visual approach, a graphical interface will be implemented.

The program will also be made more general. Nowadays the NCIPLLOT is able to read Gaussian wfn files and xyz coordinates. The interface will be expanded to other commercial/standard *ab initio* codes. In order to make it completely general, numerical derivatives will be included, so that density cube files (which are provided by basically all programs) can be read in. This will also enable to couple NCI results to other topological analysis codes (e.g. TopMod for ELF). The ultimate goal is to provide an automatized tool able to carry the analysis of all these codes.

Quantitative analysis will be made available at the local and global topological levels: localization of critical points and integrations will be implemented. Following QTAIM principles, an automated localization of critical points will be necessary in order to order different interactions in terms of their strength. At a more elaborate level, even higher order critical points could also be used to understand the connectivity among NCI regions by means of bifurcation trees. Several integration techniques will be implemented and tested for a high performing, efficient and accurate integration of NCI region.

## 3. Applications

- **High pressure chemistry:** Taking again pressure as a playground we will try to unveil the microscopic nature of high pressure processes. More specifically, I will pay attention to chlorate stability under pressure as a possible medium for CO<sub>2</sub> capture. I will also address the real space nature of electronic topological transitions, which are fundamental to understand semiconductors behavior as well as the temperature dependence of superconductors. Given the fact that these transitions are based on Fermi level changes usually associated with displacive transitions, we expect changes to occur at the valence level. As such, ELF and NCI should be appropriate tools to characterize it.
- **Ligand docking for pharmacology:** Simulation methods are playing an increasingly growing role in the design of novel drugs. An illustration is in computer-assisted drug design where *in silico* high-throughput methods can screen thousands of compounds for their affinities to a given protein target. This example illustrates both the power of contemporary computational chemistry, but also its present limitations: indeed, while several “leads” can be endowed with micromolar affinities, it is not possible (unless serendipitously) to pick out, let alone design, molecules with nano- or subnanomolar affinities, which would be really innovative and relevant for a prospective therapeutic impact. This is because the “scoring” functions (SF) are unavoidably of an empirical nature, and are unrelated to the actual inhibitor-protein intermolecular interaction energies. Yet it is these very quantities that according to thermodynamics govern the ranking of affinities of competing inhibitors to their targets. Inaccuracies in SF can generate false positives, namely compounds erroneously predicted as top scorers while their actual affinities are small, but also false negatives, namely compounds erroneously rejected because of a poor SF, while their actual affinities are high. The information obtained from Step 1 will be used to fit data sets for the development of a density-based SF.
- **Adsorption processes and heterogeneous catalysis:** Dispersion forces play a key role in the interactions between solid surfaces and the molecules present in the gas or liquid phases. The main interaction in the adsorbate-substrate system governs the composition of the interface. Such interaction may be dispersive, such as in the physisorption process, or stronger leading to dissociation (chemisorption). We will study both cases in order to understand the nature and strength of the molecule/surface system, explaining the adsorption modes that can occur. We will analyze the competition between the adsorbate-substrate and the adsorbate-adsorbate interactions, which is known

to lie at the origin of important interface phenomena such as the self-assembling of molecular layers or the physicochemical properties of meso-porous materials. Carbon chains with capping thiols and amines will be analyzed to understand these competing effects as well as the dispersion interactions among chains giving rise to the self-assembling.



**Part III**  
**Curriculum Vitae**

# Research summary

Revealing the chemical bond and its change forms the undisputed foundation of Chemistry, and it has been the focus of my scientific career following the topological approach. I devoted my thesis to the implementation and analysis of covalent bonding in the solid state in terms of the Electron Localization Function. In spite of the wide variety and binding ranges present in the solid realm, the implementation of topological analysis had remained an undone task due to the difficulties brought about by periodicity. During my thesis I implemented a new code for the complete topological analysis of ELF in solids which enabled me to apply this new tool to a whole range of solid structures, giving rise to 11 publications. They were all centered on the analysis of electron localization and its change. Thereto, I used high pressure as my playground for bond change and transformation. As an example I can cite the description of the high pressure insulating phases of metals, which gave rise to a *Phys Rev Lett*. The main results from my thesis were collected in two book chapters (one Text Book on High Pressure and one Springer book on Modern Density Analysis).

I then moved as a postdoctoral fellow at Prof Yang's group at Duke University, where I stayed for two years: firstly hired by him, working on the statistical analysis of the Chemical Universe (published in *J. Am. Chem. Soc.*) and then granted by Fulbright-RLK. During this time I returned to the Chemical bond analysis. Although there are many indexes to reveal covalent bonding, the non-covalent interactions were still a hard problem to tackle. We introduced a new index, NCI (Non Covalent Interactions) which enables visualization of non-covalent interactions, both attractive and repulsive. The index was also published in *J. Am. Chem. Soc.* in 2010 and has received over 400 citations. I also wrote the program to analyze this index, NCIPLLOT. The associated paper was published in 2011 in *JCTC* and was among the top 10 most read *JCTC* papers this year and has received over 200 citations.

Funded by the Ministry of Spain for one year, I moved to France, to the Laboratoire de Chimie Théorique (LCT). During my postdoc at LCT I established my own line on chemical bonding and electron density studies, and earned my CNRS position. I have worked on the use of electron density for understanding of carbon based materials (*Chem. Eur. J* with profile and cover) and hydrogen bonding (Top 10 most read *JCTC*). I have also developed the method for its application in reactivity and the understanding of subtle effects such as enantiomeric selectivity (*Chem. Science*) as well as the program thanks to a PhD student funded by CalSimLab. In the last years I have uniquely defined interaction volumes, within which density-based integrations can be performed to obtain properties associated solely with the interacting region. The evolution of these quantities along the potential-energy surface reproduces the interplay of attractive and repulsive interactions seen throughout hydrogen-bond formation. These results have now been collected in a chapter (Springer). The use of this index can be also found in numerous contributions to the special issue I have co-edited on "Understanding structure and reactivity from topology and beyond" (*Computational and Theoretical Chemistry-2014*).

Not forgetting my formation in solid state, I have continued my studies in materials and high pressure, which have been collected in a new book chapter (CRC Press). These studies earned me the European High Pressure Award in 2013 and also a place in the organization of the next World High Pressure meeting within the Chemistry board. On this side, I am working with a student under a co-advising agreement with Universidad de Oviedo. We are applying the chemical bond and high pressure concepts to the analysis of clatrates and CO<sub>2</sub> capture.

From the mentoring point of view, I have two PhD students (one of them under a co-advising agreement with Universidad de Oviedo). I have also had one Master student and 1 Bachelor. During this time, several students have also asked me to make short stays under my supervision (6 PhD students and 1 Master Erasmus student), showing that this line of research enables me to attract people from abroad. Even though my position is research based, I have a strong commitment to the transfer of knowledge, so I have chosen to participate in teaching in the University at all levels, from first year undergraduate to master and PhD, both at the national and international level. Analogously, I strongly believe that diffusion is a fundamental step in science. During these years I have given 29 talks, 14 of them invited. Those include 1 invitation

to WATOC and 2 invitations to Gordon Conferences. I have also chaired in 4 scientific events, including a Gordon Seminar.

# Publications

## Programs

### First author

1. NCILOT
2. CRITIC\_JAIMELF

### Corporate author

3. CRITIC2
4. NCIMILANO

## Book chapters

1. R. A. Boto, J. Contreras-Garcia in the book "Applications of Topological Methods in Molecular Chemistry" Springer
2. R. A. Boto, M. Marques, A. Beltran, J. Andres, J. Contreras-Garcia, "Chemical changes under pressure" in the book "High Pressure"
3. J. Contreras-Garcia, B. Silvi, J. M. Recio, "How ELF quantifies and pictures bonding changes along phase transitions" in the book "Modern Charge Density Analysis" Springer, 2011. ISBN 978-90-481-3835-7.
4. J. Contreras-Garcia, Jose Manuel Menendez Montes, A. Beltran, J. Andres, "Modelizacion de la Estructura y Reactividad Quimica a presiones altas", in the book "Materia a alta presion. Fundamentos y aplicaciones" Servicios de publicacion de la Universidad de Oviedo. ISBN: 978-84-8317-877-5.

## Peer-Reviewed Journals

### 2008

1. J. Contreras-Garcia, A. M. Pendas B. Silvi, J. M. Recio, "Useful Applications of the Electron Localization Function in High Pressure Crystal Chemistry", *J. Phys. Chem. Solids* 69, 2204 (2008)
2. M. Marques, J. Contreras-Garcia, M. Florez, J. M. Recio, "On the mechanism of the zircon-reidite pressure induced transformation", *J. Phys. Chem. Solids* 69, 2277 (2008)
3. J. Contreras-Garcia, A. M. Pendas, J. M. Recio, "How ELF quantifies and pictures chemical changes in a solid: the B3-B1 pressure induced phase transition in BeO", *J. Phys. Chem. B* 112, 9787 (2008)
4. G. J. Ackland, M. Marques, J. Contreras-Garcia, M. I. McMahon, "Origin of incommensurate modulations in the high-pressure phosphorus IV phase", *Phys. Rev. B* 78, 054120 (2008) [Editor's suggestion]

### 2009

5. J. Contreras-Garcia, A. M. Pendas, B. Silvi, J. M. Recio, "Bases for Understanding Polymerization under Pressure: The Practical Case of CO<sub>2</sub>", *J. Phys. Chem. B*, 113, 1068 (2009)

6. N. Barrier, J. M. Rueff, M. B. Lepetit, J. Contreras-Garcia, S. Malo, B. Raveau, "A new polymorph with a layered structure  $\epsilon$ - $\text{CaTe}_2\text{O}_5$ ", *Solid State Sciences*, 11, 289 (2009)
7. J. Contreras-Garcia, A. M. Pendas, B. Silvi, J. M. Recio, "Computation of local and global properties of the ELF topology in crystals", *J. Theor. Chem. Comp.* 113, 1068 (2009)
8. M. Florez, M. Marques, J. Contreras-Garcia, J. M. Recio, "Quantum mechanical calculations of zircon-reidite transition pathways in  $\text{ZrSiO}_4$ ", *Phys. Rev. B* 79, 104101 (2009)
9. \*J. Contreras-Garcia, J. M. Recio, "From molecular to polymeric  $\text{CO}_2$ : bonding transformations under pressure", *High Press. Res.* 29, 113 (2009)
10. M. Florez, M. Marques, J. Contreras-Garcia, J. M. Recio, "Erratum: Quantum-mechanical calculations of zircon to scheelite transition pathways in  $\text{ZrSiO}_4$ ", *Phys. Rev. B* 79, 189903(2009)
11. L. Gracia, J. Contreras-Garcia, A. Beltran, J. M. Recio, "Bonding changes across the  $\alpha$ -cristobalite  $\rightarrow$  stishovite transition path", *High Press. Res.* 29, 93 (2009)
12. A. Waskowska, L. Gerward, J. S. Olsen, M. Marques, J. Contreras-Garcia, J. M. Recio, "The bulk modulus of cubic spinel selenides: An experimental and theoretical study", *High Press. Res.* 29, 72 (2009)
13. M. Taravillo, E. del Corro, J. Contreras-Garcia, A. M. Pendas, M. Florez, J. M. Recio, V. G. Baonza, "Universal compressibility behaviour of ions in ionic crystals", *High Press. Res.* 29, 97 (2009)
14. J. Contreras-Garcia, P. Mori-Sanchez, B. Silvi, J. M. Recio, "A quantum-chemical interpretation of compressibility in solids", *J. Chem. Theor. Comp.* 5, 2108 (2009)
15. M. Marques, G.J. Ackland, L.F. Lundegaard, J. Contreras-Garcia, M.I. McMahon, "Potassium under pressure: a pseudo-binary ionic compound", *Phys. Rev. Lett.* 103, 115501 (2009)

## 2010

16. E. R. Johnson, S. Keinan, P. Mori-Sanchez, J. Contreras-Garcia, A. J. Cohen, and W. Yang, "Revealing Noncovalent Interactions", *J. Am. Chem. Soc.* 132, 6498 (2010)
17. J. T. Hammill, J. Contreras-Garcia, A. M. Virshup, D. N. Beratan, W. Yang, and P. Wipf, "Synthesis and chemical diversity analysis of bicyclo[3.3.1]non-3-en-2-ones", *Tetrahedron* 66, 5852 (2010) [**JournalCover**]

## 2011

18. \*J. Contreras-Garcia, J. M. Recio, "Electron delocalization and bond formation under the ELF framework", *Theor. Chem. Acc.* 128, 411 (2011)
19. \*J. Contreras-Garcia, J. M. Recio, "On Bonding in ionic crystals", *J. Phys. Chem. C* 115, 257 (2011)
20. J. Contreras-Garcia, E. Johnson, S. Keinan, R. Chaudret, J-P Piquemal, D. Beratan, W. Yang, "NCIPLLOT: a program for plotting non-covalent interaction regions", *J. Chem. Theor. Comp.* 7, 625 (2011) [**Top 10 most read JCTC articles 2011**]
21. M. Marques, M. Santoro, C. L. Guillaume, F. Gorelli, J. Contreras-Garcia, R. Howie, A. F. Goncharov, E. Gregoryanz, "Optical and electronic properties of dense sodium", *Phys. Rev. B* 83, 184106 (2011)
22. J. Contreras-Garcia, E. R. Johnson, W. Yang, "Analysis of Hydrogen-Bond Interaction Potentials from the Electron Density: Integration of Noncovalent Interaction Regions", *J. Phys. Chem. A* 115, 12983 (2011)

23. E. R. Johnson, J. Contreras-Garcia, "Communication: A density functional with accurate fractional-charge and fractional-spin behaviour for s-electrons.", *J. Chem. Phys. (Communication)* 135, 081103 (2011)

## 2012

24. M. Alfonso, J. Contreras-Garcia, A. Espinosa, A. Tarraga, P. Molina, "Selective Mercury (II) Cations Detection in Mixed/Aqueous Media by a Ferrocene-Based Fluorescent Receptor", *Dalton Transactions* 41, 4437 (2012)
25. T. Ouahrani, J. M. Menendez, M. Marques, J. Contreras-Garcia, V. G. Baonza, J. M. Recio "Local pressures in Zn chalcogenide polymorphs" *Eur. Phys. Soc.* 98, 56002 (2012)
26. E. R. Johnson, J. Contreras-Garcia, W. Yang, "Density-functional errors in alkanes: A real-space perspective" *J. Chem. Theor. Comp.* 8, 2626 (2012)
27. J. L. Arbour, H. S. Rzepa, J. Contreras-Garcia,\* L. A. Adrio, E. M. Barreiro, K. K. (Mimi) Hii, "Silver-Catalysed Enantioselective Addition of O-H and N-H Bonds to Allenes: A New Model for Stereoselectivity Based on Noncovalent Interactions" *Chem. Eur. J.* 18, 11317 (2012)
28. A. Otero-de-la-Roza, J. Contreras-Garcia, E. R. Johnson, "Revealing non-covalent interactions in solids, NCI plots revisited" *Phys. Chem. Chem. Phys.* 14, 12165 (2012)
29. \*J. Contreras-Garcia, M. Calatayud, J-P Piquemal, J. M. Recio, "Ionic interactions: Comparative topological approach" *Comp. Theo. Chem.* 998, 193 (2012)
30. G. Saleh, C. Gatti, L. Lo Presti, J. Contreras-Garcia, "Revealing non-covalent interactions in molecular crystals through their experimental electron densities" *Chem. Eur. J.* 18, 15523 (2012)
31. N. Gillet, R. Chaudret, J. Contreras-Garcia, W. Yang, B. Silvi, J.-P. Piquemal, "Coupling quantum interpretative techniques: another look at chemical mechanisms in organic reactions" *J. Chem. Theor. Comp.* 8, 3993 (2012)
32. X. Zheng, M. Liu, E. R. Johnson, J. Contreras-Garcia, W. Yang, "Delocalization error of density-functional approximations: a distinct manifestation in hydrogen molecular chains" *J. Chem. Phys.* 137, 214106 (2012)

## 2013

33. A. M. Virshup, J. Contreras-Garcia, P. Wipf, W. Yang, D. N. Beratan "Stochastic Voyages into Uncharted Chemical Space Produce a Representative Library of All Possible Drug-Like Compounds" *J. Am. Chem. Soc.* 135, 7296 (2013)
34. J. R. Lane, \*J. Contreras-Garcia, J.-P. Piquemal, B. J. Miller, and H. G. Kjaergaard "Are Bond Critical Points Really Critical for Hydrogen Bonding?" *J. Chem. Theory Comp.* 9, 3263 (2013) [**Most read in JCTC**]
35. R. Chaudret, B. de Courcy, J. Contreras-Garcia, E. Gloaguen, A. Zehnacker-Rentien, M. Mons, J.-P. Piquemal, "Unraveling Non Covalent Interactions within Flexible Biomolecules: from electron density topology to gas phase spectroscopy" *Phys. Chem. Chem. Phys.*, 16, 9876 (2013)

## 2014

36. J. Andres, S. Berski, J. Contreras-Garcia, P. Gonzalez-Navarrete "Following the molecular mechanism for the  $\text{NH}_3 + \text{LiH} \rightarrow \text{LiNH}_2 + \text{H}_2$  chemical reaction. A study based on the joint use of the quantum theory of atoms in molecules (QTAIM) and noncovalent interaction index (NCI)", *J. Phys. Chem.*, 118, 1663 (2014)



37. A. Armstrong, R. A. Boto, P. Dingwall, J. Contreras-Garcia, M. J. Harvey, N. Mason, H. S. Rzepa, "The Houk-List Transition states for organocatalytic mechanism revisited", *Chem. Science*, 5, 2057 (2014)
38. R. Chaudret, J. Contreras-Garcia, M. Delceya, O. Parisel, W. Yang, J.-P. Piquemal, "Revisiting H<sub>2</sub>O nucleation around Au<sup>+</sup> and Hg<sup>2+</sup>: the peculiar "Pseudo-Soft" character of the gold cation" *JCTC*, 10, 1900
39. M. Alonso, T. Woller, F. J. Martin-Martinez, J. Contreras-Garcia, P. Geerlings, F. De Proft, "Understanding the fundamental role of  $\pi$ - $\pi$ ,  $\sigma$ - $\sigma$  and  $\pi$ - $\sigma$  dispersion interactions in shaping carbon-based materials" *Chem. Eur. J.* 20, 4845 (2014) **[Cover+Profile]**
40. \*J. Contreras-Garcia, A. Otero-de-la-Roza, J. M. Recio, "El enlace quimico y su supervivencia en la Quimica Cuantica", *Anales de Quimica*, 110, 113 (2014)
41. R. A. Boto, D. Guenther, J. Contreras-Garcia, J.P. Piquemal, J. Tierny, "Characterizing Molecular Interactions in Chemical Systems", *IEEE Transactions on Visualization and Computer Graphics*, 20, 2476 (2014)

## 2015

42. F. Izquierdo-Ruiz, A. Otero-de-la-Roza, J. Contreras-Garcia, J. M. Menendez, O. Prieto-Ballesteros, J. M. Recio, "Guest-Host Interactions in Gas Clathrate Hydrates Under Pressure" *High Pressure Research*, 35, 49 (2015)
43. R. A. Boto, J. Contreras-Garcia, M. Calatayud, "The role of dispersion forces in metal-supported self-assembled monolayers" *Comp. Theo. Chem.*, 1053, 322 (2015)
44. C. Lepetit, J. Poater, M. E. Alikhani, B. Silvi, J. Contreras-Garcia, Y. Canac, M. Sola, R. Chauvin, "The Missing Entry in the Agostic-Anagostic Series: Rh(I)- $\eta^1$ -C Interactions in P(CH)<sub>3</sub>P Pincer Complexes.", *Inorg. Chem.*, 54, 2960 (2015)
45. \*J. Contreras-Garcia, M. Marques, J.M. Menendez, J.M. Recio, "From ELF to Compressibility in Solids" *Int. J. Mol. Sci.* (accepted)

## Submitted

46. G. Merino, D. Moreno, S. Pan, P. Chattaraj, J. Contreras-Garcia, J.L. Cabellos, F. Ortiz-Chi, "How Strong is a Metallocene Dimer (Metal = Fe, Ru, Os)?"
47. J. Gonzalez, I. Banos, I. Leon, J. Contreras-Garcia, E.J. Cocinero, A. Lesarri, J. A. Fernandez, J. Millan "Unravelling Protein-DNA Interactions at Molecular Level: A DFT and NCI Study"

# Conferences

## Summary:

7 scientific events organized

29 oral communications, among which

14 invited talks, one to a Gordon Conference and 1 Watoc 10 invited seminars

23 posters

4 chairings

## Organization of scientific events

1. Joint AIRAPT-25- EHPRG 53 (Madrid, 2014):Chemistry and Molecular Systems section

2. Conference : CTTC (Vietnam, 2014)
3. Conference : RCTF (Paris, 2014)
4. Training session : Hands-on session on NCI (Paris, 2013)
5. Workshop : Topological approaches to intermolecular interactions (Paris, 2013)
6. Training session : Hands-on session on NCI (Brussels, 2012)
7. Training session : Hands-on session on NCI (Paris, 2012)

## Chairwoman

1. Molecular Electrostatic Potentials Symposium (Brussels, Belgium, 2014) [Link](#)
2. Discussion Leader at Gordon Seminar (High Pressure Research) (Maine, USA, 2014)
3. Student Session: High Pressure School (Oviedo, Spain, 2013)
4. Session: Molecular crystals under pressure: Experiments and Theory (Microsymposium) EHPRG (Valencia, Spain, 2008)

## Talks

### Invited talks at conferences

1. The Chemical Bonds at the 21th Century-ICQC Satellite (Xiamen, China, 2015)[Link](#)
2. WATOC (Santiago de Chile, Chile, 2014) [Link](#)
3. Symposium in honour of Odile Eisenstein (Oslo, Norway, 2014)
4. Current Topics in Theoretical Chemistry (Vietnam, 2014) [Link](#)
5. Gordon Research Conference in High Pressure (Main, USA, 2014)
6. Journées scientifique P3M (Reims, 2013)
7. Meeting of the italian, spanish and swiss crystallographic associations (Como, Italy, 2013)
8. European High Pressure Research Group Meeting (London, UK, 2013). EHPRG Award Plenary Lecture
9. Gordon Research Conference Electron Distribution and chemical bonding (Les Diableretes, Switzerland, 2013)
10. 20th International Conference on Horizons in Hydrogen Bond Research (Antwerp, Belgium, 2013)
11. Symposium on Quantum Chemical Topology (Mexico City, Mexico, 2013)
12. Workshop " 20 years of ELF" (Paris, France, 2010)
13. Workshop "El enlace químico sin experimentos": "Non covalent interactions" (Oviedo, Spain, 2009)
14. European High Pressure Research Group Meeting (Valencia, Spain, 2008)

### Invited seminars at Universities

15. Universidad del País Vasco: "Revealing non covalent interactions" (Bilbao, 2014)
16. Université de Montpellier: "A new look at non classical hydrogen bonds: are critical points really critical for bonding?" (Montpellier, 2014)
17. Universidad de Oviedo: "Understanding the fundamental role of  $\pi$ - $\pi$ ,  $\sigma$ - $\sigma$  and  $\pi$ - $\sigma$  dispersion interactions in shaping carbon-based materials" (Oviedo, 2014)
18. Universitat de Girona: "Chemical bond indicators" (Girona, 2013)
19. Vrije Universiteit Brussel: "Non covalent interactions" (Brussels, Belgium, 2012)
20. Université Henri Poincaré Nancy 1: "Real space approaches to chemical bond" (Nancy, France, 2012)
21. LCT, Université Pierre et Marie Curie: "Les interactions non covalentes" (Paris, France, 2011)
22. University of Pittsburg: "From Density to scoring functions" (Pittsburg, USA, 2010)
23. Duke University: "Electron localization in solids" (Durham, USA, 2009)
24. Duke University: "Understanding compressibility of solids" (Durham, USA, 2007)

### Oral communications at conferences

25. Journée VISU (Paris, 2013)
26. RCTF2012: "NCI: new developments" (Marseille, France, 2012)
27. ESPA2012: "NCI: new developments" (Barcelone, Spain, 2012)
28. Journées de Modélisation: "Visualisation des interactions non covalentes" (Paris, France, 2012)

29. ACS- meeting: "From density to scoring functions: Revealing non covalent interactions" (Anaheim, USA, 2011)
30. WATOC-Satellite workshop in Materials: "Revealing non covalent interactions" (Barcelona, Spain, 2010)
31. ESPA2010: "Revealing non covalent interactions" (Oviedo, Spain, 2010)
32. SETCA2010: "Revealing non covalent interactions" (Columbia, USA, 2010)
33. 20<sup>th</sup> AIRAPT-43<sup>rd</sup> EHPRG: "Quantum mechanical simulation of pressure induced polymorphism in AgCl" (Karlsruhe, Germany, 2005)
34. IIEAP: "Aspectos termodinamicos y mecanisticos de las transiciones inducidas por presión el AgCl"(Madrid, Spain, 2004)

## Mentoring & Teaching

### Qualifications

- C.A.P. (Pedagogical training) in Chemistry (Spain, 2004-2005)
- Maître de conférences (France, 2011)
- Ayudante-Doctor (Spain, 2010)

### Mentoring

- Vanessa Riffet (ATER, UPMC, 2014-2015)
- Roberto Alvarez Boto (PhD, UPMC, 2013-2016)
- Roberto Alvarez Boto (M2-Erasmus, UPMC, 2013)
- Fernando Izquierdo Ruiz (PhD, UPMC-UNIOVI cotutelle, 2014-2017)
- Fernando Izquierdo Ruiz (M2, 2013-2014)
- Christine Anyansi (L3, Duke University, 2010-2011)

### Stages

- Zeina Maroun (3 months, University of Copenhagen, 2014)
- Tatiana Woller (6 months, VUB, 2015)

### Visiting students

- Jorge Gonzalez Rodriguez (1 week, Euskal Herriko Unibertsitatea, 2013)
- Angel Morales Garcia (1 week, Universidad Complutense de Madrid, 2014)
- David Roca Lopez (2 weeks, Universidad de Zaragoza, 2014)
- Joaquin Calbo (3 months, Universidad de Valencia, 2015)
- David Roca Lopez (2 months, Universidad de Zaragoza, 2015)

## Thesis jury

- Javier Cerezo Bastida (PhD thesis, Murcia, 2013)
- Eloy Ramos-Cordoba (PhD thesis, Girona, 2013)
- Roberto Alvarez Boto (Master thesis, Oviedo, 2013)
- Pamela Moles (PhD thesis, Castellón011)

## Teaching duties

### Undergraduate level

#### 2014-2015

- MAN Mathematics and Physics (36 hours TD, University Paris-Descartes)
- Chemistry (30 hours Cours+TD, Universidad de Oviedo)

#### 2013-2014

- Physics (48 hours TD PCEM1, University Paris-Descartes)
- Theoretical Chemistry (30 hours TD, U. Paris-Descartes)

#### 2012-2013

- Theoretical Chemistry (12 hours TD, ENSTA)
- Theoretical Chemistry (12 hours TD, U. Paris-Descartes)
- TIC-Physics (10.5 hours TP L1, University Paris-Descartes)
- TIC-Internet (10.5 hours TP L1, University Paris-Descartes)
- Calculus Support (15 hours Cours L1, University Paris-Descartes)

#### 2011-2012

- TIC-Physics (10.5 hours TP L1, University Paris-Descartes)
- TIC-Internet (10.5 hours TP L1, University Paris-Descartes)
- Calculus Support (15 hours Cours L1, University Paris-Descartes)

### PhD/Master level

#### 2014-2015

- Spanish Master Program in Solid State Chemistry (10 hours, Zaragoza)
- Master Label IdF/Nord du RCTF (3 hours Cours+3hours TD, Paris)

#### 2012-2013

- Ecole d'été Maths-Chimie-HPC 2013 (Roscoff)
- High Pressure School (5 hours, Oviedo)

#### 2011-2012

- Master Program in Solid State Chemistry (10h, Zaragoza)

#### 2006-2007

- High Pressure School (2h, Barcelona, 2007)

## Awards and Recognitions

### Awards

- European High Pressure Research Group Award (2013)
- Best thesis in Chemistry at the University of Oviedo by the Chemistry Association (2009)
- Prix of Excellence PhD in Chemistry at the the University of Oviedo (2009)

- Prix of Excellence Licenciatura (College) in Chemistry at the the University of Oviedo (2004)
- Best student in the promotion 2003 in Chemistry at the University of Oviedo (2003)
- Excellence in Erasmus (2002)
- Prix of Excellence at Bachillerato (High School) of Asturias (1999)
- Matricula de Honor in COU (preparatory year for University) (1998)

## **Grants**

- Postdoctoral grant from the Spanish Ministry of Education (2010)
- Fulbright "Occasional lecturer fund" (2009)
- Fulbright - Ruth Lee Kennedy grant (2009)
- High Performance Computing grant for Paris (2009)
- F.P.U. (PhD grant) by the Spanish Ministry of Education (2004)
- Erasmus grant for North London University (2001)

# **Responsibilities**

## **Editor responsibilities**

Special Issue of Computational and Theoretical Chemistry on "Understanding structure and reactivity from topology and beyond". Handling Editor: Manuel Yanez. Guest Editors: Angel Marting Pendas and Julia Contreras-Garcia

## **Referee responsibilities**

- Chemical Physics
- Journal of Chemical Physics
- Theoretical Chemistry Accounts
- Molecular Physics
- Computational and Theoretical Chemistry

## **Project Referral for international academies**

- Research Foundation Flanders (FWO)
- Agencia Nacional de Evaluacion y Prospectiva (ANEP)

**Part IV**  
**Appendix**



## Appendix

**Parameters for promolecular calculations.** Parameterized exponents ( $\eta_i$ ) and coefficients ( $c_i$ ) of sphericalized atomic densities, in atomic units.

Atom	$c_1$	$\eta_1$	$c_2$	$\eta_2$	$c_3$	$\eta_3$
H	0.2815	0.5288	—	—	—	—
He	2.437	0.3379	—	—	—	—
Li	11.84	0.1912	0.06332	0.9992	—	—
Be	31.34	0.1390	0.3694	0.6945	—	—
B	67.82	0.1059	0.8527	0.5300	—	—
C	120.2	0.0884	1.172	0.5480	—	—
N	190.9	0.0767	2.247	0.4532	—	—
O	289.5	0.0669	2.879	0.3974	—	—
F	406.3	0.0608	3.049	0.3994	—	—
Ne	561.3	0.0549	6.984	0.3447	—	—
Na	760.8	0.0496	22.42	0.2511	0.06358	1.0236
Mg	1016	0.0449	37.17	0.2150	0.3331	0.7753
Al	1319	0.0411	57.95	0.1874	0.8878	0.5962
Si	1658	0.0382	87.16	0.1654	0.7888	0.6995
P	2042	0.0358	115.7	0.1509	1.465	0.5851
S	2501	0.0335	158.0	0.1369	2.170	0.5149
Cl	3024	0.0315	205.5	0.1259	3.369	0.4974
Ar	3625	0.0296	260.0	0.1168	5.211	0.4412



